

國立交通大學
光電工程研究所
碩士學位論文

非同步鎖模光纖光固子雷射之雷射動力
學

**Laser Dynamics of Asynchronous Mode locked
Fiber Soliton Lasers**



研究生：張宏傑

指導教授：賴暎杰

中華民國九十七年七月

非同步鎖模光纖光固子雷射之雷射動力學
Laser Dynamics of Asynchronous Mode locked Fiber Soliton Lasers

研究生：張宏傑

Student : Hon-Chieh Chang

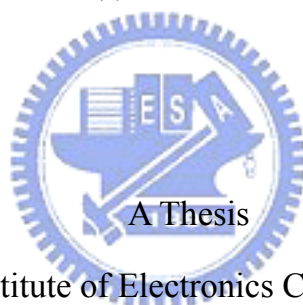
指導教授：賴暎杰 老師

Advisor : Yin-Chieh Lai

國立交通大學

光電工程研究所

碩士論文



Submitted to Institute of Electronics College of Engineering

National Chiao Tung University

in partial Fulfillment of the Requirements

for the Degree of

Master

In Electro-Optical Engineering

July 2008

Hsinchu, Taiwan, Republic of China

中華民國九十七年七月

摘要

論文名稱：非同步鎖模光纖光固子雷射之雷射動力學

校所別：國立交通大學光電工程研究所

頁數：1 頁

畢業時間：九十七學年度第二學期

學位：碩士

研究生：張宏傑

指導教授：賴暎杰 老師

非同步鎖模光纖光固子雷射有著令人感興趣的特性，例如：脈衝參數的慢速週期性變化，良好的低雜訊表現等。它們應該可以應用在高速光通訊，超快光處理，和其他科學上的研究。本論文之主旨在研究如何以藉由直接分析雷射輸出光脈衝序列之電子頻譜圖來獲得有關脈衝時間位置和脈衝中心頻率的慢速週期性變化之振幅大小，從而可與理論分析與模擬結果來作比較。透過這樣的研究，我們得以深入了解非同步鎖模光固子雷射之特性並發展其應用。

ABSTRACT

Title : Laser Dynamics of Asynchronous Mode locked Fiber Soliton Lasers

Pages : 1 Page

School : National Chiao Tung University


Department : Institute of Electro-Optical Engineering

Time : July, 2008

Degree : Master

Researcher : Hon-Chieh Chang

Advisor : Prof. Yin-Chieh Lai



Asynchronous mode-locked fiber soliton lasers have some interesting properties including slow periodic variation of the pulse parameters and excellent low noise performance. They may find applications in high speed optical communication, ultrafast optical processing, and other scientific researches. The study of the thesis is focused on how to characterize the slow periodic variation of the pulse timing position and the pulse center frequency by directly analyzing the RF spectra of the laser output pulse train. The measured results are compared with theoretical results to enhance our understanding on the laser dynamics of asynchronous mode locked fiber soliton lasers. This will also help to develop the applications of this new laser source.

ACKNOWLEDGEMENT

在這兩年的碩士生涯中，首先要特別對我的指導教授 賴暎杰老師在研究的過程中不斷的給予支持與耐心的指導表達敬意與感謝之意，使我在求學的過程中受益良多。

特別要感謝 項維巍老師，這兩年來在生活上的照顧與作實驗期間細心和不厭其煩的教導，並適時給我鼓勵。感謝 林俊廷學長的熱心指導，使得我的實驗能順利完成。感謝 陳南光學長、徐桂珠學姐、許宜襄學姐和施伯宗學長課業和實驗上的指教。另外感謝實驗室的同學 佩綦、偉哲、易辰、文智、盛鵬、芳銘、文強、宸瑋，與他們的交討與討論，讓我在課業上、實驗上，與相關領域的了解，獲益匪淺，以及在生活上彼此的幫忙照應；感謝學弟妹 昱勳、子翔、佩芳、漢昇、士愷、昱宏、小咨、彥林等人的熱情支持與打氣，讓我在這兩年的實驗室生涯中豐富色彩，謝謝所有幫助過我的人。

最後要感謝父母和家人的支持和鼓勵，讓我能順利的完成碩士學業。

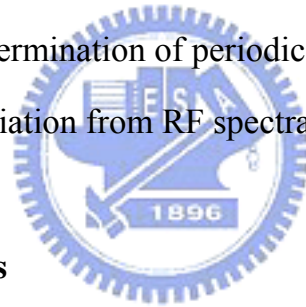
CONTENTS

	Page
Abstract (in Chinese)	i
Abstract (in English)	ii
Acknowledgement	iii
Contents	iv
List of Figures	vi
Chapter 1 : Introduction	
1.1 Overview	1
1.2 Motivation	3
1.3 Thesis organization	4
References	5
Chapter 2 : Theories of mode-locked lasers	
2.1 Pulse characteristics	6
2.1-1 Gaussian pulses	7
2.1-2 Hyperbolic secant pulses	8
2.2 Active mode-locked lasers	10
I. Amplitude modulation (AM) mode-locking	11
II. Phase modulation (PM) mode-locking	13
2.3 Passive mode-locked lasers	17
I. Nonlinear amplifying loop mirror (NALM)	18
II. Saturable absorbers	19
III. Polarization additive pulse mode-locking (P-APM)	20

2.4 Hybrid mode-locked lasers	22
2.5 Asynchronous mode-locked lasers	23
References	26

Chapter 3 : Experimental setup and results

3.1 The 10GHz ASM Er-fiber soliton laser	27
3.1.1 Experimental setup and component parameters	27
3.1.2 Experimental results	30
3.2 Pulse dynamics of ASM fiber soliton lasers	34
3.2.1 Variational analysis	34
3.2.2 Determination of periodic pulse timing position	36
variation from RF spectra	
3.2.3 Determination of periodic pulse center frequency	42
variation from RF spectra	
References	48



Chapter 4 : Conclusions

4.1 Summary	49
4.2 Future work	50

LIST OF FIGURES

Fig. 2.1	Shapes of Gaussian and sech pulse.....	9
Fig. 2.2	Schematic setup of an active mode-locked laser	10
Fig. 2.3	Active mode-locking process in the frequency domain	11
Fig. 2.4	Active mode-locking process in the time domain	12
Fig. 2.5	Development of pulse train in time domain by superposition of modes	14
Fig. 2.6	Time domain of phase modulation	15
Fig. 2.7	Schematic setup of a passive mode-locked laser	17
Fig. 2.8	Basic parts of the NALM.....	18
Fig. 2.9	Schematic of the time dependence of pulse and net gain with fast saturable absorber	19
Fig. 2.10	Schematic of the time dependence of the net gain window with slow saturable absorber	20
Fig. 2.11	Schematic of how pulse shortening occurs in a laser through P-APM.....	21
Fig. 2.12	Schematic of the asynchronous soliton mode-locked laser	23
Fig. 2.13	The noise-cleanup effect in the asynchronous soliton mode-locked laser	24
Fig. 3-1	Experiment setup.....	27
Fig. 3-2	The optical spectrum. The bandwidth is 5.4 nm directly from the laser cavity	30
Fig. 3-3	The RF spectrum (center near 10 GHz, span 50 MHz)	30
Fig. 3-4	The RF spectrum (span 500 kHz, deviation frequency: 25.5 kHz)	31

Fig. 3-5	The RF spectrum (span 500 kHz, deviation frequency: 35 kHz)	31
Fig. 3-6	The RF spectrum (span 500 kHz, deviation frequency: 47 kHz)	32
Fig. 3-7	The RF spectrum (span 500 kHz, deviation frequency: 54 kHz)	32
Fig. 3-8	Autocorrelation of the pulses	33
Fig. 3-9	Slow periodic evolution of the pulse parameters: (a) pulse timing position, (b) pulse center frequency, (c) pulse energy, (d) pulse-width	35
Fig. 3-10	The pulse train signals in the time domain	36
Fig. 3-11	The pulse train signals in the frequency domain	37
Fig. 3-12	Schematic of observed the frequency sub-components	37
Fig. 3-13	The frequency sub-components on the RF spectrum.....	38
Fig. 3-14	RF spectrum near 10 GHz (Span: 750 kHz)	39
Fig. 3-15	RF spectrum near 20 GHz (Span: 750 kHz)	40
Fig. 3-16	RF spectrum near 30 GHz (Span: 750 kHz)	40
Fig. 3-17	RF spectrum near 40 GHz (Span: 750 kHz)	41
Fig. 3-18	Schematic of pulse center frequency and pulse timing position variation.....	42
Fig. 3-19	Schematic of measuring the pulse timing position variation without and with the SMF 28 fiber.....	43
Fig. 3-20	RF spectrum near 10 GHz with 0 m SMF 28 fiber (Span: 500 kHz)	44
Fig. 3-21	RF spectrum near 10 GHz with 50 m SMF 28 fiber	

	(Span: 500 kHz)	45
Fig. 3-22	RF spectrum near 10 GHz with 100 m SMF 28 fiber	
	(Span: 500 kHz)	45
Fig. 3-23	RF spectrum near 10 GHz with 200 m SMF 28 fiber	
	(Span: 500 kHz)	46
Fig. 3-24	RF spectrum near 10 GHz with 300 m SMF 28 fiber	
	(Span: 500 kHz)	46
Table. 3-1	The devices in the fiber ring cavity.....	29
Table. 3-2	The parameters of the mode-locked laser	39
Table. 3-3	The ratios of the RF intensity at mf_H to that at	
	$mf_H + \Delta f$ from m=1 to m=4	41
Table. 3-4	The parameters of the mode-locked laser	44
Table. 3-5	The ratios of the RF intensity and the estimated	
	wavelength variation	47

Chapter 1

Introduction

1.1 Overview

The first fiber laser was demonstrated in 1961 based on a Nd-doped fiber with 300 μm and high loss [1.1] and low-loss silica fibers were first used to build diode-pumped fiber lasers in 1973. However, it was not until the late 1980s that fiber lasers began to attract a lot of research interest. The initial emphases of the research were on Nd and Er-doped fiber lasers, but fiber lasers with other dopants such as holmium, samarium, thulium, and ytterbium have also been studied. Nd-doped fiber lasers are of considerable practical interest since they can be pumped by GaAs semiconductor lasers operating near 0.8 μm . On the other hand, Er-doped fiber lasers can operate in several wavelength regions, ranging from visible to infrared. The 1.55 μm wavelength region has attracted the most attention because it coincides with the low-loss region of silica fibers for optical communication applications.

The method of locking the multiple axial modes in a laser cavity is called mode-locking. It can also be used to mode-lock fiber lasers in which the rare-earth-doped fibers are acting as the gain medium. Mode-locked fiber lasers can be made very long, up to several kilometers, which allows for low repetition rates. Several groups have reported mode locking of neodymium-doped and erbium-doped fiber lasers. Geister and Ulrich built the first integrated system using a lithium niobate phase modulator and obtained 90ps pulses at 1080nm [1.2]. Up to date, the shortest pulse width obtained from a mode-locked fiber laser was shorter than 100fs.

Mode-locked fiber lasers are ideal light sources for fiber-optic communication due to their device compactness, fiber compatibility, and better quality (almost transform-limited short pulses compared to those from laser diodes). Fiber-type

devices have the benefits such as lower coupling loss and simplicity for manufacturing by splicing as well as achievable significant nonlinear effects from small core area and long interaction length. Mode-locked fiber lasers can generate short pulses at the high repetition rate by employing mode-locking mechanisms to establish the fixed relationship among the phase of the different frequency components (modes).

Typically, we have two popular ways to achieve mode-locking; one is active mode-locking and the other is passive mode-locking. Active mode-locking can generate pulse trains at higher repetition rates when compared with passive mode-locking. On the other hand, passive mode-locking can generate shorter pulses when compared to active mode-locking. To generate shorter pulses at high repetition rate together, hybrid mode-locking can be used by employing the two methods together.

However, there are still some issues to be solved. One of these issues is that fiber lasers are affected easily by environmental perturbations due to their fiber-type nature. In active mode-locking, synchronization between the harmonic component of the cavity frequency and the modulation frequency must be perfectly kept for achieving stable mode-locking. It is not easy to do in practice since the ambient temperature fluctuations will cause the length of the fiber cavity to change thermally. The cavity frequency harmonic components drift and the synchronicity is no longer maintained. Particularly, longer cavity length causes larger variation, which is further enlarged at higher harmonics. Thus some cavity length stabilization schemes are needed to be implemented to maintain the synchronization for long term operation.

As said above, one needs high speed feedback electronics for stabilizing typical synchronous mode-locked fiber lasers, but these electronics are expensive for economic practice. If we use the asynchronous mode-locking scheme, the feedback stabilization in fact can be achieved more easily by detuning the modulation frequency

of the phase modulator slightly off the cavity harmonic frequency by 10~50 kHz. In this way, the 10~50 kHz spectral beating components around DC in the RF spectrum can be used to carry out a more economic stabilization scheme with the use of only kHz electronics. One of the merits of asynchronous mode-locked fiber lasers is thus that they can be stably operate at a very high repetition rate and generate very short pulses at the same time with less cost.

Recently asynchronous soliton model-locking has been shown to be an effective technique for generating ultrashort pulses with GHz repetition rates [1.3, 1.4]. 10 GHz 0.8 ps mode-locked Er-fiber lasers in the 1.55 μ m regime have been successfully demonstrated [1.4]. These 10 GHz sub-ps pulses directly from the laser output should have high potentials for applications in high speed optical communication, ultrafast optical processing and other scientific researches.



1.2 Motivation

The asynchronous mode-locked fiber soliton lasers have many interesting properties: slow periodic variation of pulse parameters, excellent low noise performance. They may find applications in high speed optical communication, ultrafast optical processing and other scientific researches. In this thesis work we try to characterize these properties experimentally and theoretically. In particular, we focus on the experimental determination of the actual magnitude of the timing position variation and the center wavelength variation. We also want to compare the experimental results with theoretical prediction to enhance the understanding of the laser dynamics of this new laser source.

1.3 Thesis organization

This thesis is consisted of four chapters. Chapter 1 is an overview of fiber lasers and our motivation for doing this research. Chapter 2 describes the theory of mode-locked fiber lasers including the active mode-locking, passive mode-locking, hybrid mode-locking, and asynchronous mode-locking. Chapter 3 presents the experimental setup and results. Analyses of the results are also included. Finally chapter 4 gives a summary about the achievements and future prospects of the work done here.



Reference

- [1.1] E. Snitzer, “Optical maser action of Nd in a barium crown glass”, Physical review letters, 7,444(1961).
- [1.2] P.W. France, “Optical fiber lasers and amplifiers,” 1991.
- [1.3] C.R. Doerr, H.A. Haus, and E.P. Ippen, “Asynchronous soliton mode locking”, Opt. Lett. 19, 1958 (1994).
- [1.4] W.-W Hsiang, C.-Y Lin, M.-F Tien, and Y. Lai, “Direct generation of a 10 GHz 816 fs pulse train from an erbium-fiber soliton laser with asynchronous phase modulation,” Opt. Lett. 30, pp. 2493-2495 (2005).



Chapter 2

Theories of mode-locked lasers

2.1 Pulse characteristics

Optical pulses or typical optical pulse trains from mode-locked lasers can be characterized in diverse respects:

1. The pulse width can be measured by an autocorrelator or a streak camera. Optical sampling techniques can be used when a shorter reference pulse is available.
2. The pulse repetition rate is usually measured by a high speed photodiode and a RF spectrum analyzer.
3. The pulse energy may be (for pulse trains) calculated from the repetition rate and the average power or directly measured.
4. The peak power may be calculated from pulse energy, pulse width and pulse shape or measured directly by a photodiode.
5. The optical center frequency and spectral shape can be obtained by an optical spectrum analyzer.
6. The timing jitter of a pulse train can be measured by diverse methods including the RF spectral domain method or the time domain sampling method.
7. The coherence can be characterized by an interferometer.
8. The chirp can be inferred from the optical spectrum and pulsewidth measurements for the simplest cases.
9. The carrier-envelope offset phase is of special interest for few cycle pulses and can be characterized by the autocorrelator.

There are also methods of complete pulse characterization [2.1], which can infer the

complex spectrum (including spectral phase and spectral shape) of ultrashort pulses or the electric field versus time. The simplest mathematical function from of the pulses is either in the form of hyperbolic secant or Gaussian, which is a solution to the master equation for passive or active mode-locked lasers.

2.1.1 Gaussian pulses

The function form of the most general Gaussian optical pulse is written [2.2] as bellows:

$$E(t) = \frac{1}{2} E_0 \exp[-\gamma t^2] \exp(j\omega_p t) \quad (2.1)$$

$$\gamma = \alpha - j\beta \quad (2.2)$$

Where α : describes the width of the Gaussian pulse

ω_p : the carrier frequency

β : governs the frequency chirp of such pulse

The bandwidth or spectral width (Δf_p) of the pulse is defined as the frequency separation between the two half-power points of the optical spectra and is given by

$$\Delta f_p = \frac{1}{\pi} \sqrt{\frac{2 \ln 2 (\alpha^2 + \beta^2)}{\alpha}} \quad (2.3)$$

The pulsewidth (τ_p) is defined as the time separation between the two half-intensity points and is given by

$$\tau_p = \sqrt{\frac{2 \ln 2}{\alpha}} \quad (2.4)$$

It is known that the Fourier transform of a Gaussian function is still a Gaussian

function, so the optical spectra can be written as:

$$E(\omega) = \frac{E_0}{2} \sqrt{\frac{\pi}{\gamma}} \exp\left(\frac{-(\omega - \omega_p)^2}{\alpha}\right) \quad (2.5)$$

From Equation (2.3) and (2.4) the pulse-bandwidth product parameter for Gaussian pulses can be derived. It is often used to characterize pulses, under the Gaussian pulse assumption. The pulse-bandwidth product can be written as:

$$\tau_p \Delta f_p = \left(\frac{2 \ln 2}{\pi}\right) \sqrt{1 + \left(\frac{\beta}{\alpha}\right)^2} \quad (2.6)$$

For chirpless Gaussian pulses ($\beta = 0$), $\tau_p \Delta f_p = 0.44$.

2.1.2 Hyperbolic secant pulses

The hyperbolic secant pulse has the following function forms

$$E(t) = E_0 \operatorname{sech}\left(\frac{t}{\tau}\right) \exp(j\omega_p t) \quad (2.7)$$

The Fourier transform of a hyperbolic secant function is also a hyperbolic secant:

$$E(\omega) = E_0 \tau \sqrt{\frac{\pi}{2}} \operatorname{sech}\left(\frac{\tau \pi \omega}{2}\right) \quad (2.8)$$

The pulsewidth (τ_p) is give by

$$\tau_p = \tau \ln \frac{\sqrt{2} + 1}{\sqrt{2} - 1} \cong 1.763 \tau \quad (2.9)$$

and the bandwidth (Δf_p) is :

$$\Delta f_p = \frac{1}{\tau \pi^2} \ln \frac{\sqrt{2} + 1}{\sqrt{2} - 1} \quad (2.10)$$

The time-bandwidth product is $\tau_p \Delta f_p = 0.314$ for chirpless pulses.

The following figure describes the difference between hyperbolic secant and Gaussian pulses. It is noticed that the wings of Gaussian pulses is smaller than the wings of sech pulses.

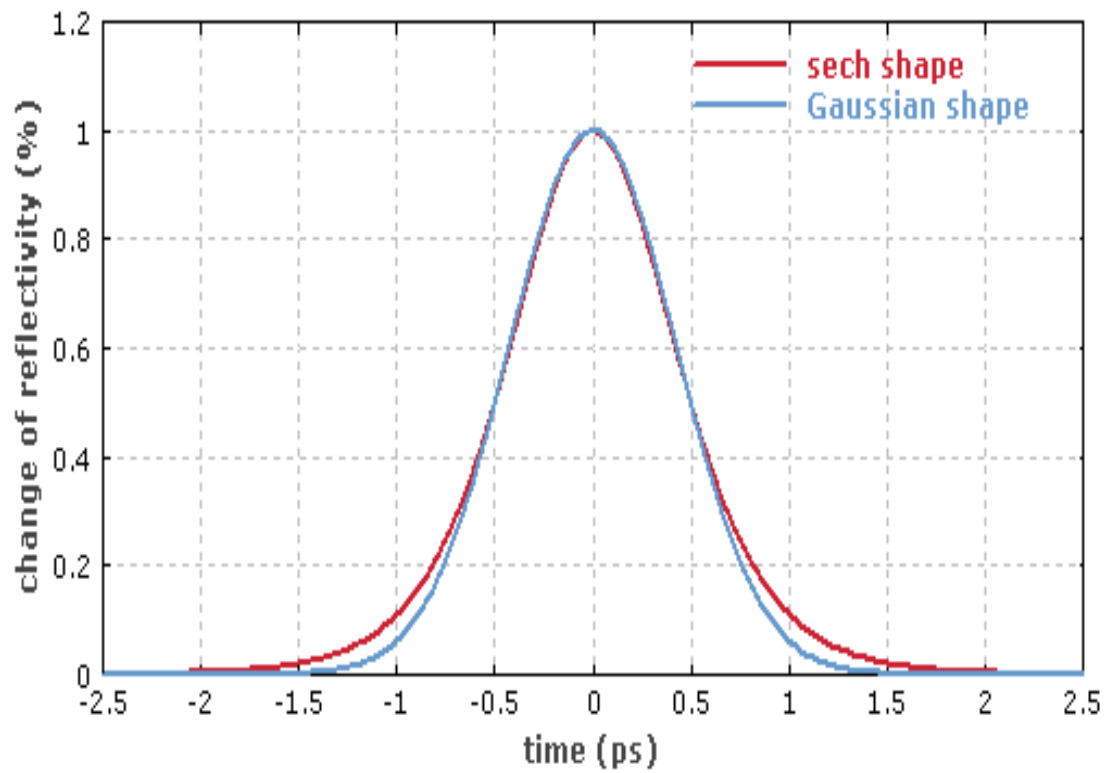


Fig. 2.1 Shapes of Gaussian and sech pulse

2.2 Active mode-locked lasers

Active mode locking can be performed by introducing periodic modulation of the resonator losses or of the round-trip phase change. This can be achieved with a Mach–Zehnder integrated-optic modulator, a semiconductor electroabsorption modulator or an acousto-optic or electro-optic modulator. If the modulation is synchronized with the resonator round trips, light pulses in synchronization with the modulation can continue to grow and mode locking is achieved.

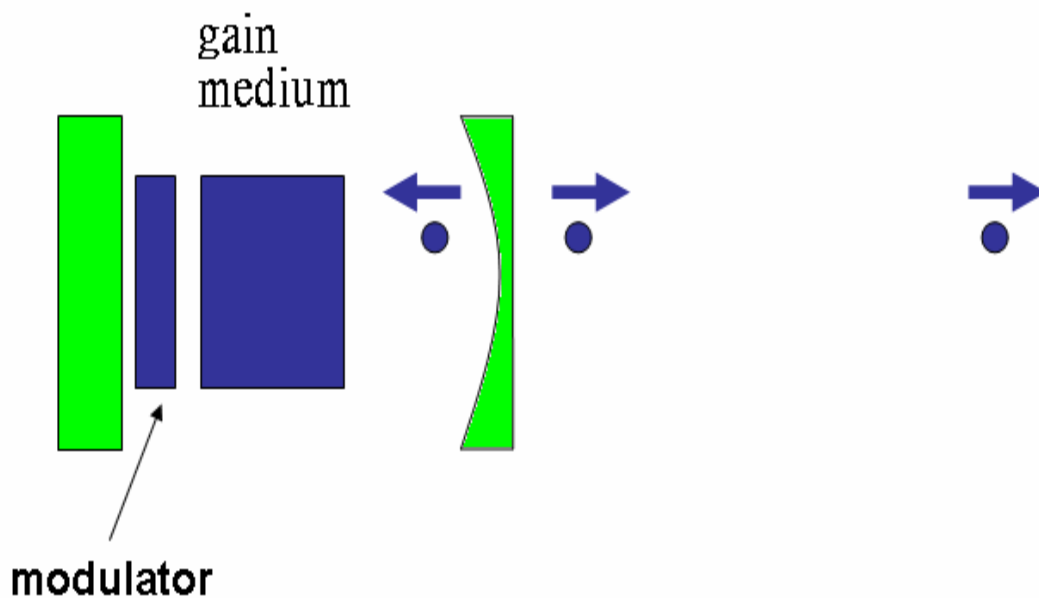


Fig. 2.2 Schematic setup of an active mode-locked laser

Typically, active mode-locked laser has two general methods of modulation. One is Amplitude modulation (AM) mode-locking, and the other is Phase modulation (PM) mode-locking. A detailed introduction for the two general methods of modulation will be given in the following sections.

I. Amplitude modulation (AM) mode-locking

Amplitude modulation mode-locking is a way to generate a short pulse train with high repetition rate by modulating directly the optical amplitude. It can be analyzed both in the frequency and time domains [2.3].

A laser is formed by introducing a gain medium inside a cavity and has axial modes separated in frequency by $\Delta\Omega = \frac{2\pi}{T_R}$, where T_R is the round-trip time. In the frequency domain, several axial modes will be lasing if the gain level is above threshold. Denote the frequency of the central mode by ω_0 . If the laser is mode-locked by the amplitude modulator placed near one of the mirrors (see Fig. 2.2), and then a cosinusoidal modulation of the central mode at the frequency $\Omega_M = N\Delta\Omega$ generates sidebands at $\omega_0 \pm \Omega_M$. These sidebands can injection-lock the adjacent modes in succession and finally the mode-locking is achieved. Figure 2.3 shows the active mode-locking process in the frequency domain with $N=1$.

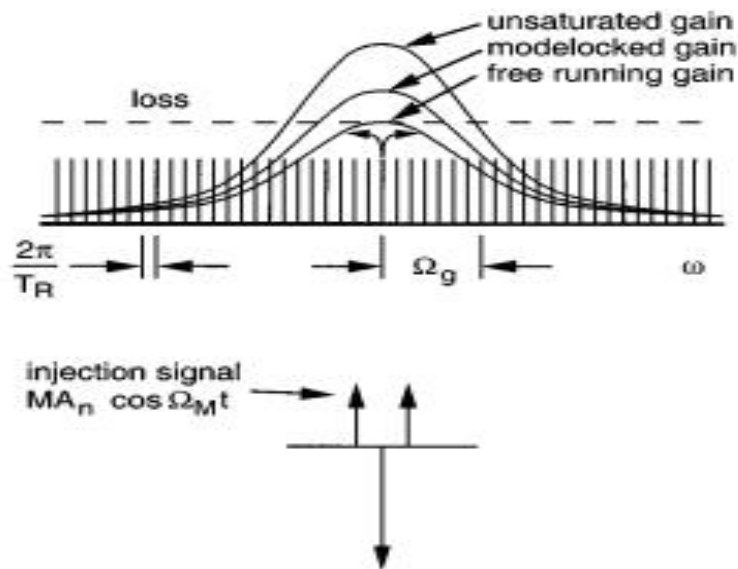


Fig 2.3 Active mode-locking process in the frequency domain [2.3]

In the time domain, the amplitude modulation provides a time dependent loss so that only the pulses that pass through the modulator at the lowest loss will exist. As the modulation period is matched to the cavity round-trip time, the light which is incident at one particular point in the modulation cycle will be incident at the same point after one round trip of the cavity. Thus any light that suffered a loss after one round trip will always experience a loss. All the lights in the cavity will experience a net loss except those which pass through the modulator around the zero loss point. Figure 2.4 shows the active mode-locking process in the time domain.

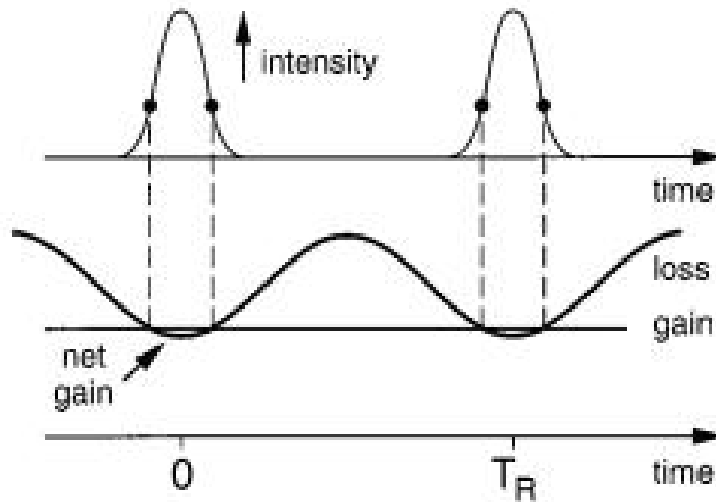


Fig 2.4 Active mode-locking process in the time domain [2.3]

The master equation of amplitude modulation mode-locked lasers is written as:

$$T_R \frac{\partial a(T,t)}{\partial T} = (g-l)a(T,t) + \frac{g}{\Omega_g^2} \frac{\partial^2}{\partial t^2} a(T,t) - \frac{1}{2} M \Omega_M t^2 a(T,t) \quad (2.11)$$

Where g : the saturated gain per pass

l : the loss

Ω_g : the gain bandwidth

M : the modulation index

The amplitude of the central mode without amplitude modulation is expressed as:

$$E(t) = E_0 \cos(\omega_0 t) \quad (2.12)$$

After passing the amplitude modulator, the light field can be written as:

$$\begin{aligned} E(t) &= E_0 (1 + M \cos \Omega_M t) \cos(\omega_0 t) \\ &= E_0 \cos(\omega_0 t) + E_0 \frac{M}{2} \cos(\omega_0 - \Omega_M) + E_0 \frac{M}{2} \cos(\omega_0 + \Omega_M) \end{aligned} \quad (2.13)$$

The modes that are separated every Ω_M will be phase-locked, and short pulses can be formed in the time domain. When $N=1$, the laser is mode locked at the fundamental repetition rate. As $N > 1$, the laser is harmonic mode locked. The Fourier transform of equation (2.11) is written as:

$$T_R \frac{\partial A(T, \Omega)}{\partial T} = (g - l)A(T, \Omega) - g \frac{\Omega^2}{\Omega_g^2} A(T, \Omega) + \frac{1}{2} M \Omega_M \frac{\partial^2 A(T, \Omega)}{\partial \Omega^2} \quad (2.14)$$

Where $A(T, \Omega)$ is the Fourier transform of $a(T, t)$. Generally, its solution can be expressed in terms of Hermite-Gaussians functions.

$$A(T, \Omega) = \sum_n C_n(T) H_n(\Omega \tau) \exp\left(\frac{-\Omega^2 \tau^2}{2}\right) \quad (2.15)$$

II. Phase modulation (PM) mode-locking

Phase modulation mode-locking is a way to generate a short pulse train with a high repetition rate by modulating the optical phase. It can also be analyzed both in frequency and time domains [2.4].

In the frequency domain, we can assume that the central frequency is ω_0 . When it passes through the phase modulator, the electric field of the pulse can be written as:

$$\begin{aligned}
E(t) &= E_0 \cos(\omega_0 t + M \cos(\Omega_M t)) \\
&= E_0 \sum_{-\infty}^{\infty} J_n(M) \cos(\omega_0 t + n\Omega_M t) \quad (2.16)
\end{aligned}$$

When Ω_M : the modulating frequency of phase modulator

M : the modulation index

J_n : the n-th order Bessel function

The master equation of phase modulation mode-locked lasers can be written as:

$$T_R \frac{\partial a}{\partial T} = (g - l)a + \frac{g}{\Omega_g^2} \frac{d^2 a}{dt^2} + jM \cos(\Omega_M t)a \quad (2.17)$$

If Ω_M is N times magnitude of the fundamental harmonic frequency of the cavity and ω_0 is one of the harmonic modes in the laser cavity, these harmonic modes ($\omega_0 + K\Omega_M$) will have the fixed phase relation with the ω_0 , where $K = \pm 1, \pm 2, \pm 3, \dots$, etc. Thus, all these harmonic modes will have fixed phase relation by injection-locking. In the time domain, these harmonic modes will create constructive interference at periodic time and destructive interference at other time. This is shown in Figure 2.5.

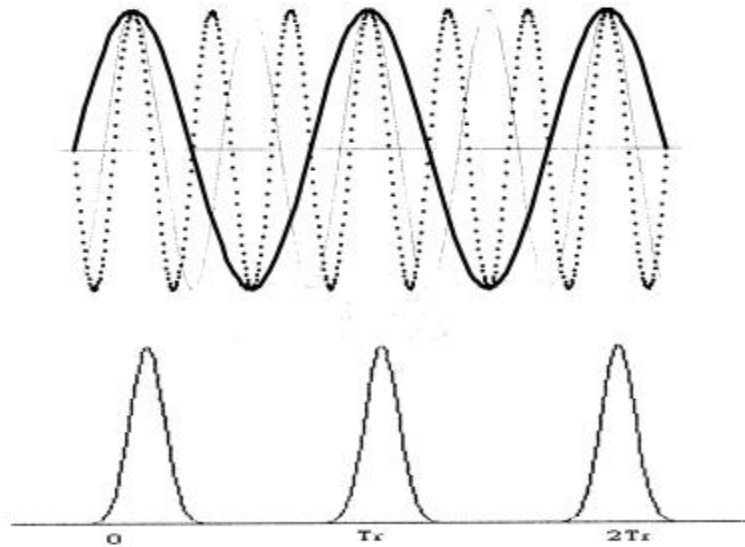


Figure 2.5 Development of pulse train in time domain by superposition of modes

In the time domain, the phase modulator provides a periodic phase change for the optical pulse. If the pulsewidth is much smaller than the modulation period, then the optical phase change generated by the phase modulator can be expressed as:

$$\phi(t) = \varphi_0 + \frac{d\varphi}{dt}t + \frac{d^2\varphi}{dt^2}t^2 + \dots \quad (2.18)$$

The term φ_0 is a constant, so it has no influence on optical pulses. The first order term $\frac{d\varphi}{dt}t$ will influence the central frequency of the pulses and the shifting magnitude of influence depends on its value. Therefore, when the pulses pass through the PM modulator, the central frequency will be shifted and in turn the pulse will experience smaller gain. Hence, if $\frac{d\phi}{dt} \neq 0$, the central frequency of optical pulse will be changed. In another word, if $\frac{d\phi}{dt}$ is still not equal to zero, the pulse will experience smaller gain and the center frequency will still be changed. This is unstable and the pulse will not last. Only the pulses which pass through the PM modulator at $\frac{d\phi}{dt} = 0$ every roundtrip are able to be stable. This is shown in Figure 2.6.

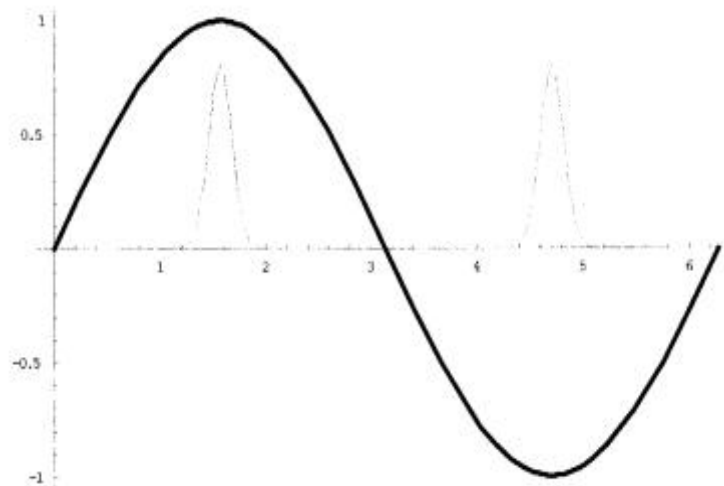


Fig 2.6 Time domain of phase modulation

As regarding the second order term $\frac{d^2\varphi}{dt^2}t^2$, it adds a chirp to the pulse and will affect the optical bandwidth of the pulses. The effect can be expressed in mathematics by:

$$\Delta\omega = \sqrt{\frac{1}{\tau^2} + \eta\tau^2} \quad (2.19)$$

Where $\Delta\omega$: the bandwidth of optical pulse

τ : the pulsewidth

$\eta = \frac{d^2\varphi}{dt^2}$: the chirp parameter



2.3 Passive mode-locked lasers

Passive mode-locking uses all-optical nonlinear techniques and is able to generate ultrashort optical pulses without any active component (such as a modulator) in the laser cavity [2.5]. This is illustrated in figure 2.7.

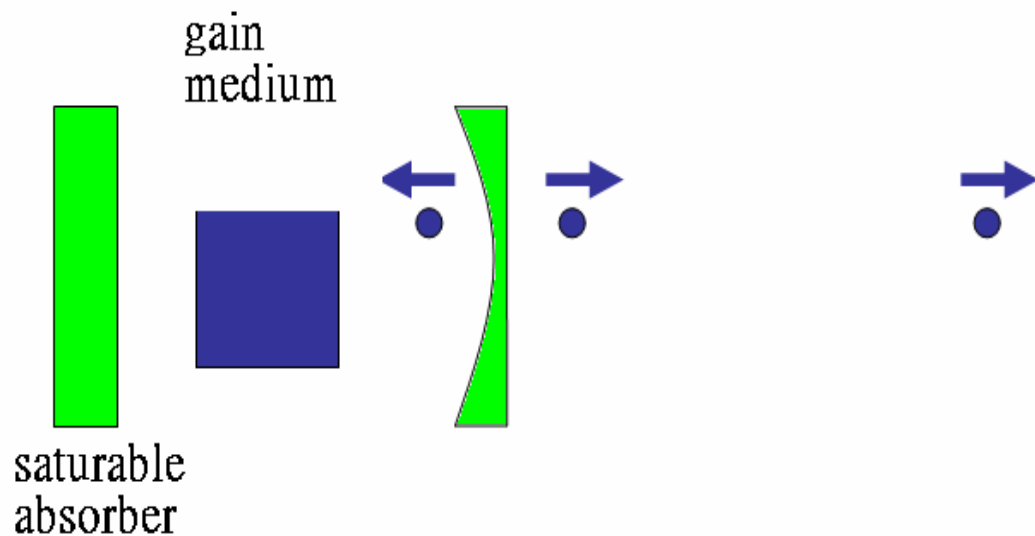


Fig. 2.7 Schematic setup of a passive mode-locked laser

It makes use of nonlinear optical devices whose response to the entering optical pulse is intensity dependent. Up to now, many methods for implementing of passive mode-locking have been proposed and demonstrated for building passively mode-locked fiber lasers. Passive mode-locked lasers to generate subpicosecond pulses has been achieved using three main methods: nonlinear amplifying loop mirror, nonlinear polarization rotation (also called polarization additive pulse mode-locking), and saturable absorbers. These methods will be introduced in the following sub-sections.

I. Nonlinear amplifying loop mirror (NALM)

The NALM relies on the Kerr effect in a length of optical fiber in conjunction with polarizers to cause artificial saturable absorber action and achieve pulse shortening [2.5]. The NALM consists of a fiber Sagnac interferometer with the gain section placed asymmetrically in the loop. A differential phase shift occurs between the lights in the two directions of the NALM, and with proper phase bias the NALM transmits higher intensities while reflecting low intensities. The NALM is attached to a unidirectional fiber ring, forming a figure-8 shaped cavity where the reflected low intensities are then extinguished by the isolator in the unidirectional ring. As the pulse energy is increased, SPM (self-phase modulation) will produce phase imbalance for the two counterdirectional pulses inside the loop. This is shown in figure 2.8.

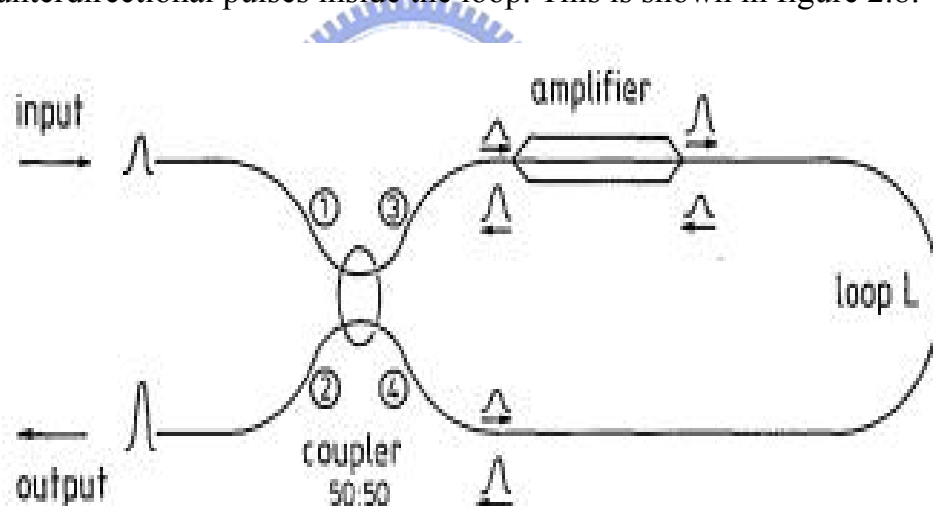


Fig. 2.8 Basic parts of the NALM [2.6]

The nonlinear reflectivity of the NALM also can serve as an all-optical switch for femtosecond pulses.

II. Saturable absorbers

Saturable absorbers have been used for passive mode-locking since the early 1970s. The basic mechanism in nearly all the passive mode-locked lasers is the pulse shortening effect caused by the transmission through a saturable absorber element. This is shown in figure 2.7.

There are two types of saturable absorbers, fast and slow absorbers. The main difference is the relation of the relaxation time and the pulse width. The relaxation time is much shorter than the pulse width for the fast saturable absorber. On the contrary, the relaxation time of the slow saturable absorber is much longer than the pulse width.

When the relaxation time is much shorter than the pulse width, the absorber can respond immediately. The laser gain is approximately time independent and the net gain window is fully dependent on the input optical pulse width. When an optical pulse propagates through such an absorber, its wings experience more loss than the central part which is intense enough to saturate the absorber. This is shown in figure 2.10. Therefore, the optical pulse will be shortened after the passage through the absorber and ultimately the laser will be mode-locked.

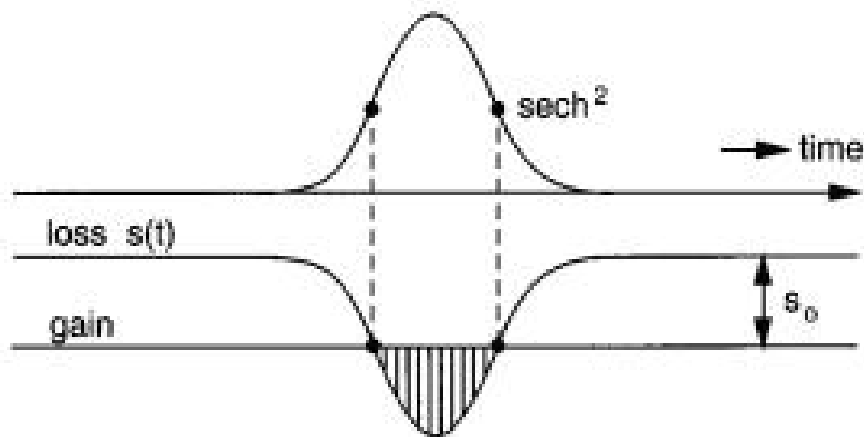


Fig. 2.9 Schematic of the time dependence of pulse and net gain with fast saturable absorber [2.3]

As the relaxation time is much longer than the pulse width, the absorber can not respond immediately to recover to the initial loss within the duration of the optical input pulse. It is possible to achieve the pulse shortening effect by combining with the dynamic laser gain. This is shown in figure 2.11.

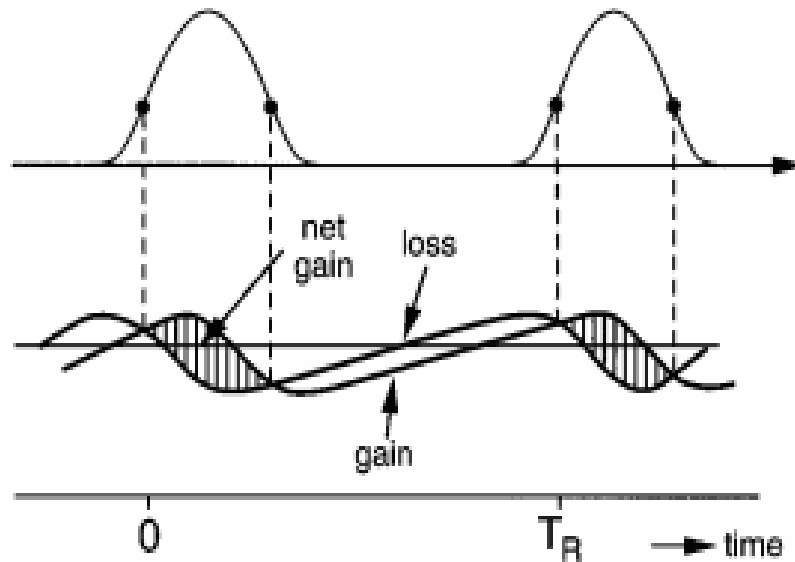


Fig. 2.10 Schematic of the time dependence of the net gain window with slow saturable absorber [2.3]

III. Polarization additive pulse mode-locking (P-APM)

Additive pulse mode-locking (APM) is a passive mode-locking technique that utilizes the nonlinear interference effect between the two pulses inside the cavity to achieve pulse shortening. Both pulses are phase modulated by SPM to different extent so that constructive interference occurs around the peak, which leads to low loss, while destructive interference at both tails, which leads to high loss. The APM mechanism does not impose a practical limit on the shortest and has been extended to fiber lasers, where the pulse shortening is achieved by polarization control and SPM.

“Polarization-APM”, or “Nonlinear Polarization Rotation” is one method of

implementing APM [2.7] Nonlinear polarization rotation can occur in an optical fiber when the initial polarization state is elliptical. The ellipse can be decomposed into right-hand and left-hand circular polarization components with different intensities. SPM from the isotropic Kerr medium modulates the phase unequally so that the ellipse rotates with maintained handedness and ellipticity. The nonlinear polarization rotation can also be used in conjunction with bulk polarization optics to obtain an artificial saturable absorber for mode-locking. The mode-locking technique called “Nonlinear Polarization Rotation Mode-locking” adds two polarization components together at the polarizer where the peak of the pulse with more rotation transmits at low loss and the wings are blocked. This is shown in figure 2.11.

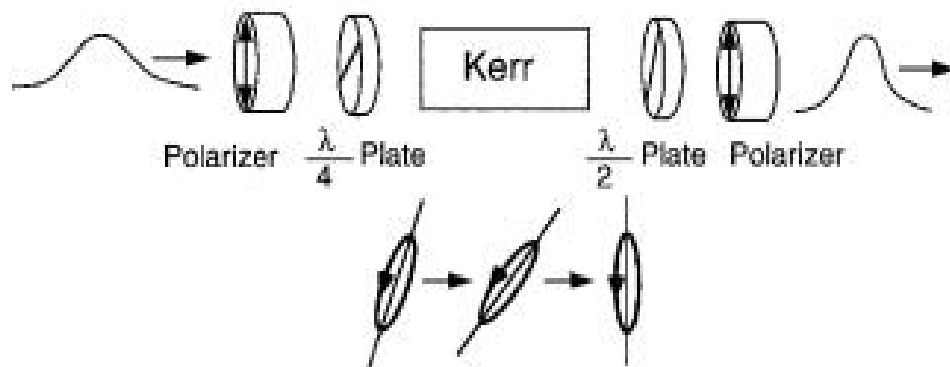


Fig. 2.11 Schematic of how pulse shortening occurs in a laser through P-APM [2.5]

2.4 Hybrid mode-locked lasers

Hybrid mode-locking combines multiple mode-locking techniques within the same laser cavity to improve the laser performance [2.4]. The Hybrid mode-locking usually incorporates the active mode-locking with passive mode-locking. The combination puts an amplitude or phase modulator inside a passively mode-locked fiber laser. The active mode-locking mechanism produces a pulse train with a high repetition rate and the passive mode-locking mechanism shortens the pulse to the fs level. An alternative hybrid mode-locking method is to add a real slow saturable absorber in a cavity which is also using a fast saturable absorber. The slow saturable absorber can easily generate a picosecond pulses to be helpful for initiating mode-locking (self-starting capability) [2.8].



2.5 Asynchronous mode-locked lasers

In the normal active mode-locked lasers, the optical modulator is driven synchronously. In the other words, the modulation frequency is equal to the cavity harmonic frequency accurately. Under the condition of synchronization, the pulses in the laser cavity reach the optical modulator at the center of the modulation signal to achieve stable mode-locking. However, in the asynchronous soliton mode-locked lasers [2.10], the modulation frequency and the cavity harmonic frequency have a deviation frequency form several kHz to tens kHz. For the normal linear optical pulses, they are affected by the several kHz frequency shifts, and are unable to achieve stable mode-locking. But the soliton pulses with the nonlinear effects, it not only can achieve the stable mode-locking under the appropriate conditions but can get the shorter pulse (<1 ps). The mechanism of asynchronous soliton mode-locking is illustrated in Figure 2.12.

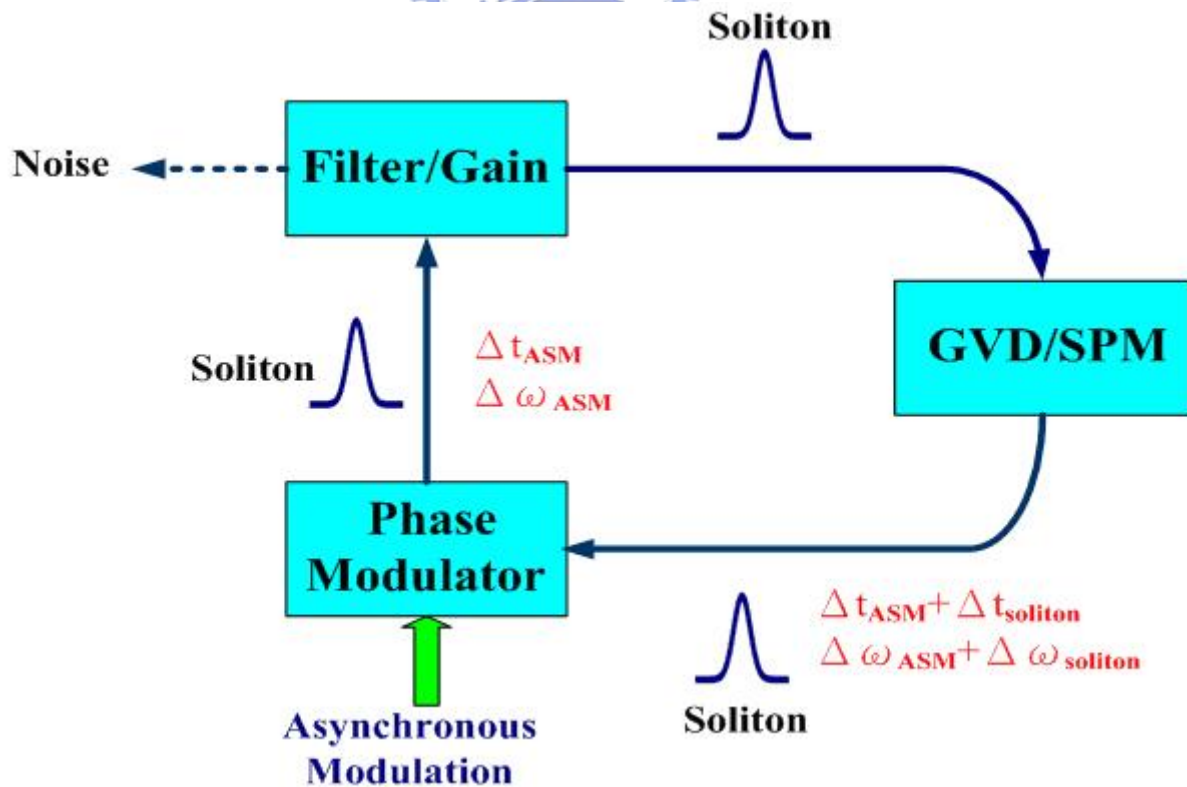


Fig. 2.12 Schematic of the asynchronous soliton mode-locked laser.

The fiber laser is consisted of the gain, the optical bandpass filter, group velocity dispersion (GVD), self-phase modulation (SPM), and the phase modulator driven asynchronously. Because of asynchronous modulation, the time of the pulse reaches the optical modulator does not always fix at the center of the modulation signal. When the pulse passes through the phase modulator, the central wavelength of the pulse can get a small shift. When the nonlinear effects are not considered, the asynchronous modulation constantly shifts the central frequency of the pulse with accumulation. Because the gain medium and the filter are both fixed with finite bandwidth, the overdeveloped amount of the central frequency shift can make the pulse leave the center of the gain or the filter, the pulses will experience quite large loss and can not exist in the cavity, as is shown in Figure 2.13.

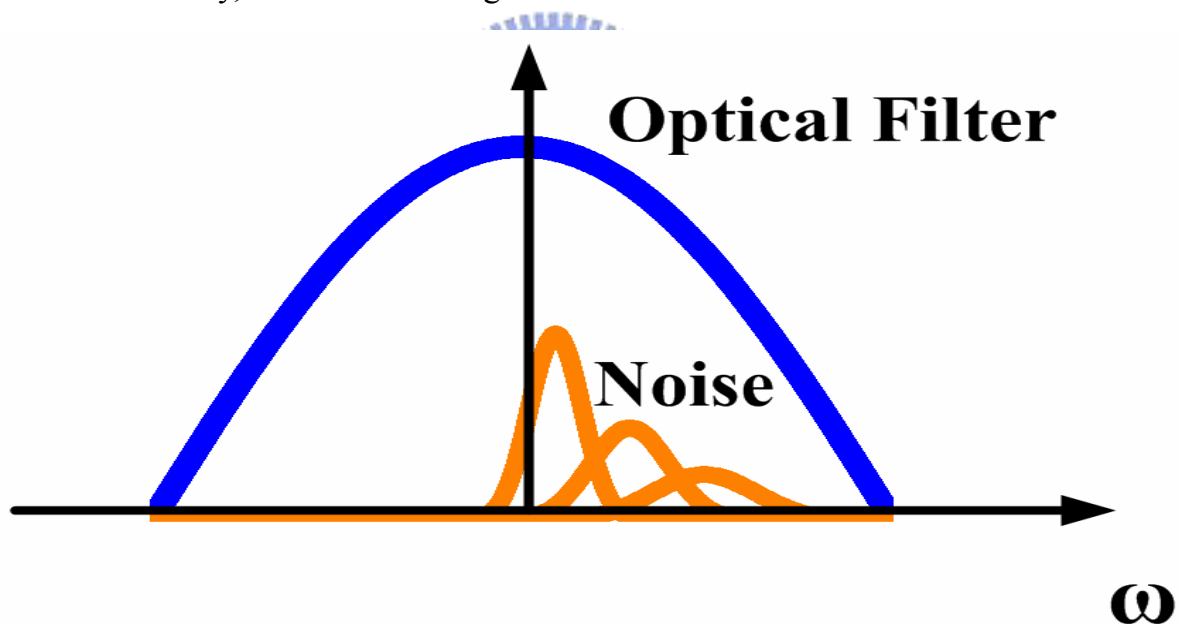


Fig. 2.13 The noise-cleanup effect in the asynchronous soliton mode-locked laser.

Contrarily, the solitons produced by the Kerr nonlinear effects can react against the frequency shift produced by the asynchronous modulation. So the solitons will experience smaller loss and can exist steadily in the cavity.

The mechanism explained above is similar to the effects of the sliding-frequency

guiding filter [2.11] in the soliton communication systems. The central frequency of the soliton can change with the variation of the center frequency of the filters in the fiber link when propagating, but the center frequency of the linear noise keeps fixed and will be filtered out by the sliding filters. In the asynchronous soliton mode-locking, it achieves the similar noise-cleanup effects with the fixed center frequency of the filter and the sliding center frequency of the soliton.



Reference

- [2.1] I. A. Walmsley and V. Wong, "Characterization of the electric field of ultrashort optical pulses", *J. Opt. Soc. Am. B* 13 (11), 2453 (1996)
- [2.2] Dirk J. Kuizenga and A. E. Siegman, "FM and AM mode locking of the homogeneous laser-Part I:Theory" *IEEE J. Quantum Electronics*, vol. 6, no. 11, pp. 694-708 (1970)
- [2.3] Herman A. Haus, "Mode-locking of Lasers", *IEEE J.on Selected topics in Quant. Electron.* 6, 1773(2000)
- [2.4] M.C. Chan, "Hybrid mode-locking Er-Fiber Laser", Institute of Electro-Optical engineering in National Chiao-Tung University, master thesis (2002)
- [2.5] L.E. Nelson, D.J. Jones, K. Tamura, H.A. Haus, E.P. Ippen, "Ultrashort-pulse fiber ring lasers" *Appl. Phys. B* 65, 277-294 (1997)
- [2.6] FERMAN, M. E., et al. "Non-linear amplifying loop mirror" *Opt. Lett.*, 15, pp. 752-754 (1990)
- [2.7] H. A. Haus, E.P. Ippen, and K. Tamura, "Additive-Pulse Modelocking in Fiber Lasers", *IEEE J. Quantum Electronics*, vol. 30, no. 1, pp. 200-208 (1994)
- [2.8] Siegman Anthony E, "Lasers," 1986.
- [2.9] H. A. Haus, D.J. Jones, E.P. Ippen, and W.S. Wong, "Theory of soliton stability in asynchronous mode-locking," *IEEE J. Lightwave Technology* 14, 622, 1996.
- [2.10] C. R. Doerr, H.A. Haus, and E.P. Ippen, "Asynchronous soliton mode locking", *Opt. Lett.* 19, 1958 (1994).
- [2.11] L. F. Mollenauer, J. P. Gordon, and S. G. Evangelides, "The sliding-frequency guiding filter: an improved form of soliton jitter control" *Opt. Lett.*, 17, 1575(1992)

Chapter 3

Experimental setup and results

3.1 The 10GHz ASM Er-fiber soliton laser

3.1.1 Experimental setup and component parameters

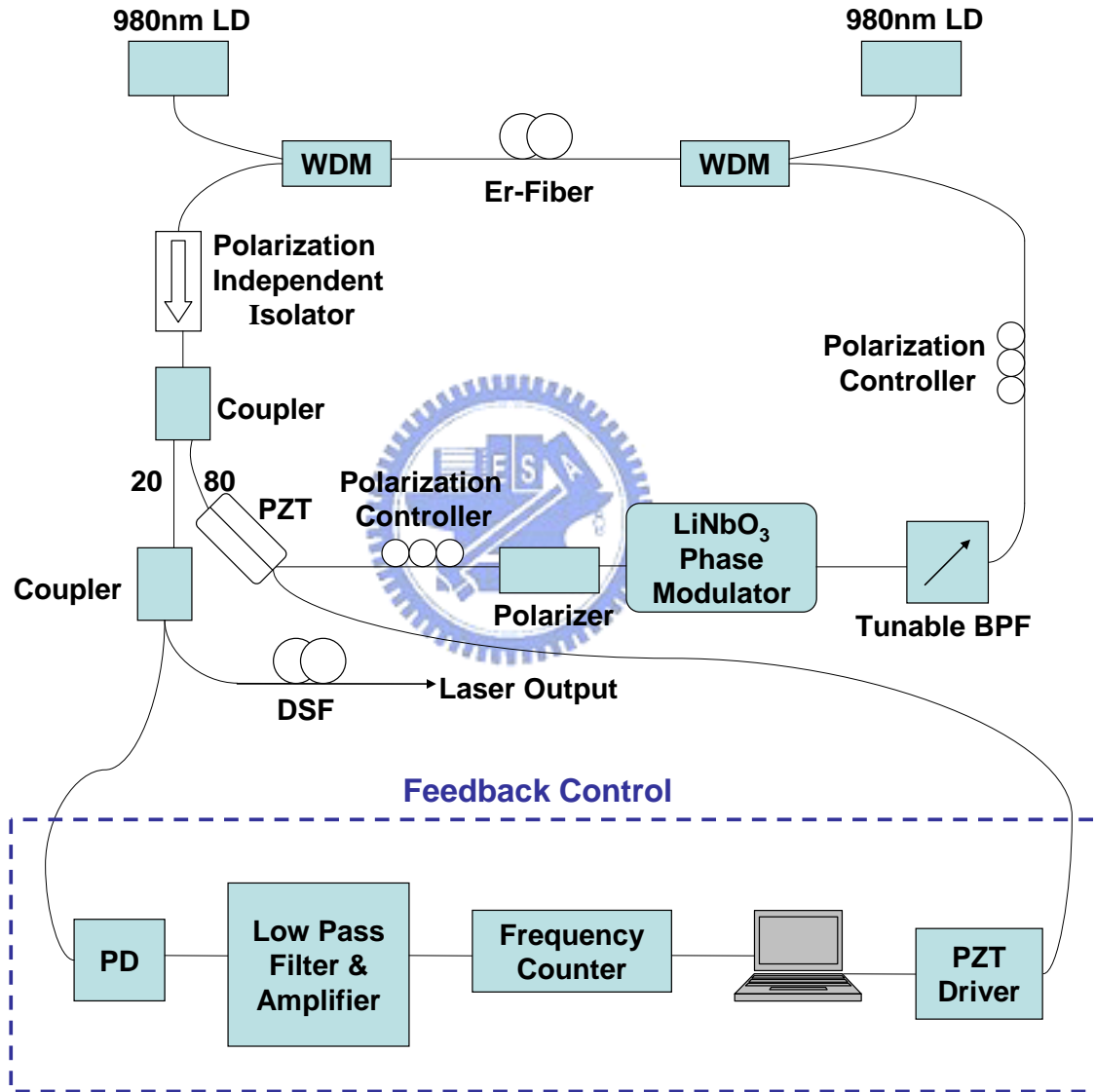


Fig. 3.1 Experiment setup

The experimental setup of our ASM Er-fiber soliton laser is shown in the figure above. In our experiment, we use the technique of hybrid mode-locking. We put an EO

phase modulator into the cavity of a passive mode-locked laser and keep the setup all-fiber. The phase modulator needs a polarizer in the input end to align the polarization axis of pulses with that of the EO crystal. The isolator is for single direction wave propagation to prevent spatial hole burning and is polarization-independent since the polarizer and the phase modulator provides enough polarization dependent loss for Polarization Additive Pulse Mode-locking (P-APM). The two polarization controllers are placed in the cavity to adjust the polarization state for achieving P-APM. In order to get more nonlinearity in the fiber cavity, high intra-cavity light intensity is needed. As a result, the method of bi-directional pumping is utilized in the experimental setup and about 350 mW of 980 nm pump is used in the experiment. An EO phase modulator is put in the fiber ring cavity to achieve active mode-locking. If the EO modulator is replaced with a polarization dependent isolator, the laser becomes a purely passive mode-locked laser.

The tunable bandpass filter is used to select the lasing wavelength of the laser. In addition, it can cooperate with the self-phase modulation (SPM) effect in the cavity to suppress supermodes and to achieve a high supermode suppression ratio (SMSR). Besides, the wide bandwidth of the bandpass filter can support shorter pulses in the cavity so that the generated pulse width also can be shorter.

A section of 5.5 meters Erbium-doped fiber pumped by two 980 nm laser diodes acts as the gain medium of our laser. The output coupler is put behind the Er-fiber to get the greatest output power. The coupling ratio is 80/20 to couple 20% power inside the laser to the laser output. The chirp of the pulses is compensated with a length of negative group-velocity dispersion (GVD) fiber.

The feedback control circuit as shown in figure 3.1 is used to stabilize the asynchronous mode-locked laser. It is composed of a photo detector, a low pass filter, an amplifier, a frequency counter, a computer, a PZT driver, and a PZT. The signal

obtained from the photo detector is amplified by the amplifier, and filtered out the unnecessary signals by the low pass filter, then the signals we want are sent to the frequency counter is delivered to the computer. The PZT driver controlled by the LABVIEW software of the computer applies the voltage on the PZT, to change the cavity length for stabilizing the mode-locked laser. The devices that have been used in the fiber ring cavity are list in table 3.1.

Table 3.1 The devices in the fiber ring cavity

1.	980nm pump laser : maximum output power : 602mA x 1 : 450mA x 1
2.	EO phase modulator
3.	Tunable bandpass filter: 3dB bandwidth: 13.5 nm ; central wavelength:1530~1570 nm
4.	Polarization independent isolator x 2
5.	WDM coupler (980 nm/ 1550 nm) x 2
6.	PM fiber : located at the EO phase modulator
7.	Erbium-doped fiber: about 5.5 M
8.	Dispersion shifted singlemode fiber: about 2M
9.	Single mode fiber: about 19.33 M
10.	Coupler: 80/20 x 1; 95/5 x 1
11.	Polarization controller x 2
12.	Photo detector
13.	Amplifier
14.	Low pass filter: frequency 500 Hz to 64000 Hz
15.	Frequency counter: frequency DC to 225 MHz
16.	PZT driver: voltage 0 V to 150 V
17.	PZT

3.1.2 Experimental results

We have achieved several excellent experimental results. First, the optical bandwidth of our laser output is about 5.0 nm. This is shown in figure 3.2.

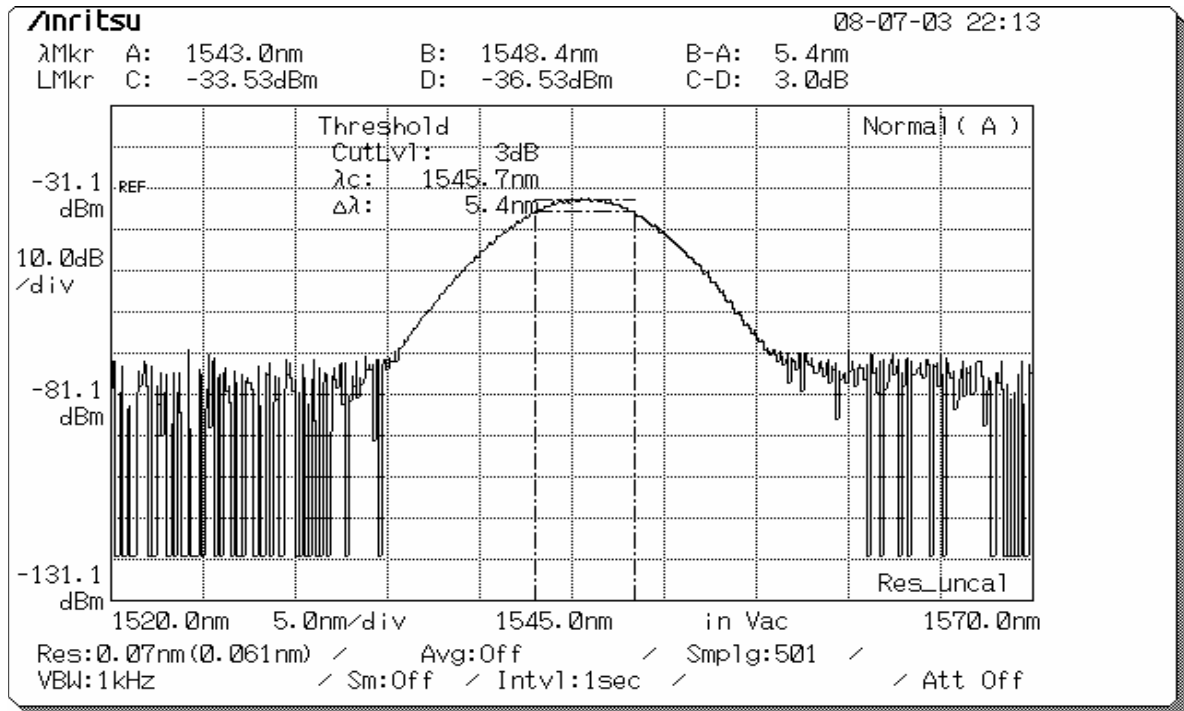


Fig. 3.2 The optical spectrum. The bandwidth is 5.4 nm directly from the laser cavity.

Second, the SMSR is greater than 70 dB. This is shown in figure 3.3.

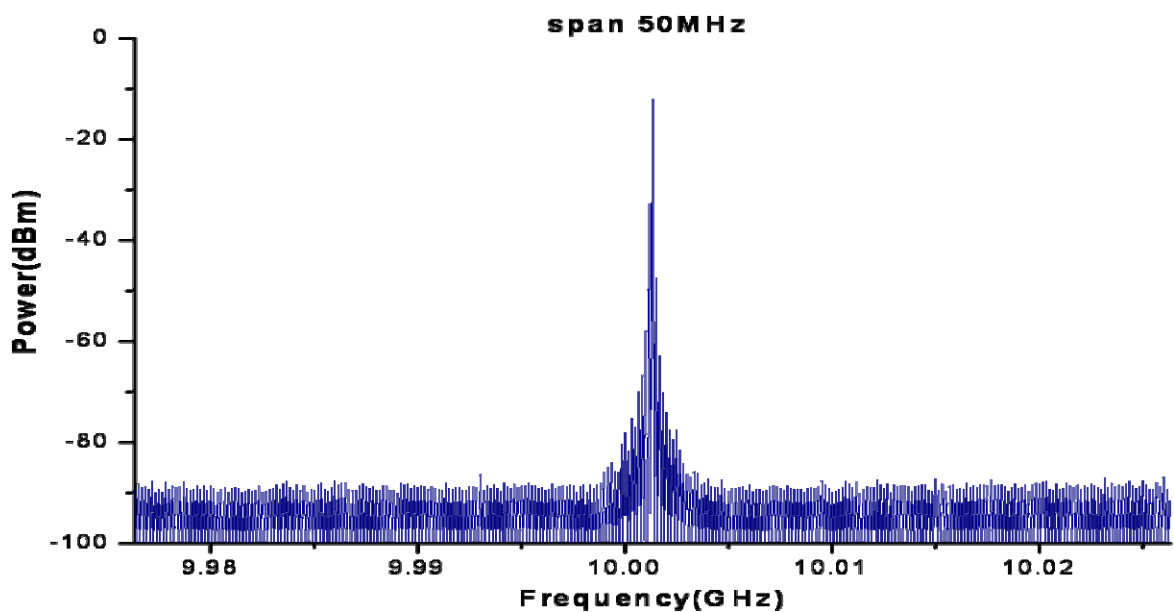


Fig. 3.3 The RF spectrum (center near 10 GHz, span 50 MHz)

Third, under the situation of asynchronous mode-locking, the range of the deviation frequency (difference of the cavity harmonic frequency and the modulation frequency) is found to 10 kHz ~ 60 kHz. These are shown in figure 3.4, figure 3.5, figure 3.6 and figure 3.7 respectively.

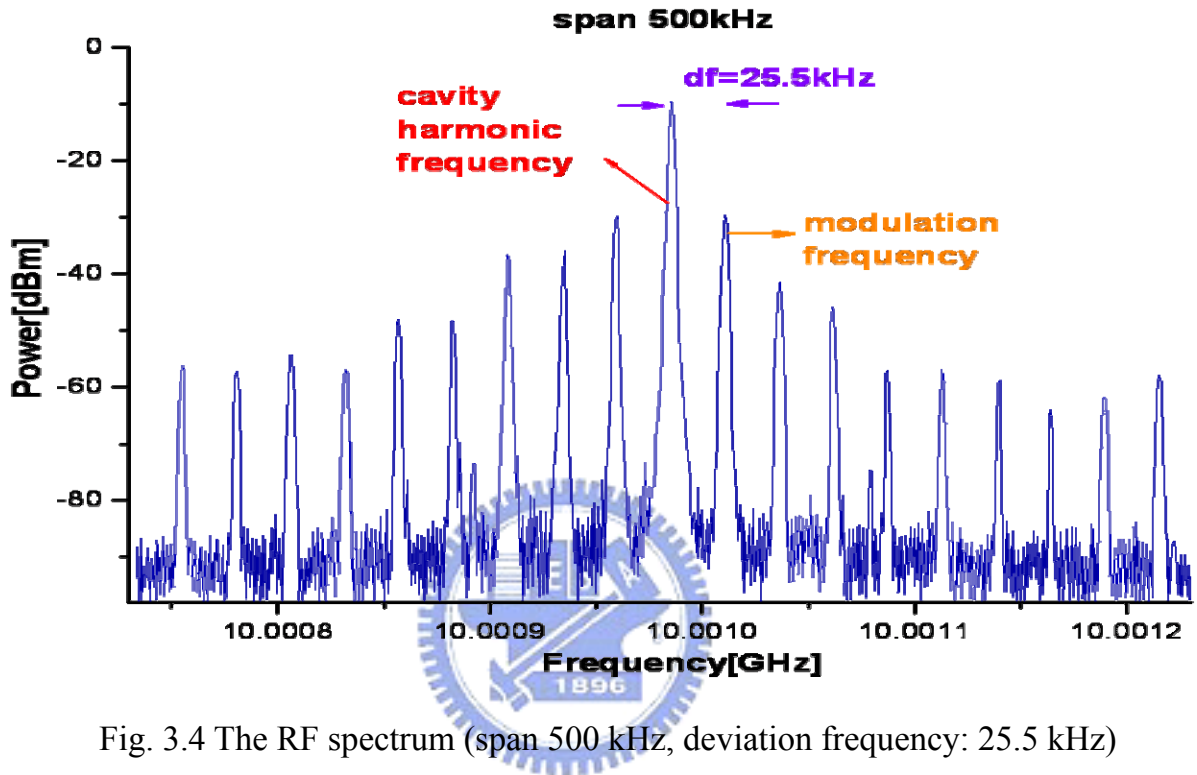


Fig. 3.4 The RF spectrum (span 500 kHz, deviation frequency: 25.5 kHz)

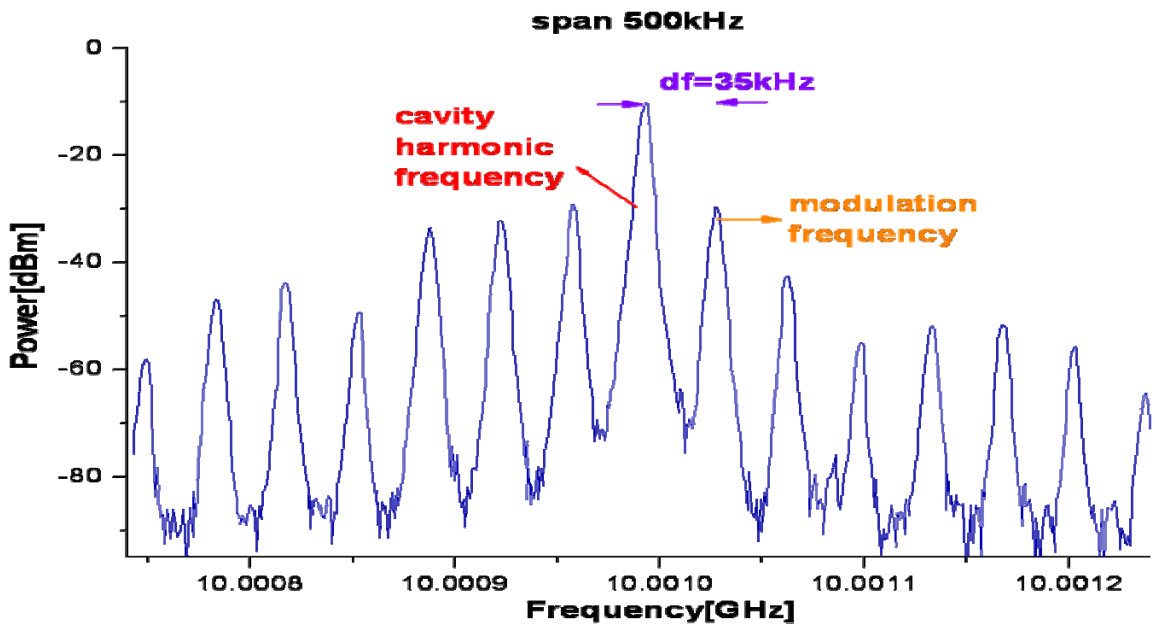


Fig. 3.5 The RF spectrum (span 500 kHz, deviation frequency: 35 kHz)

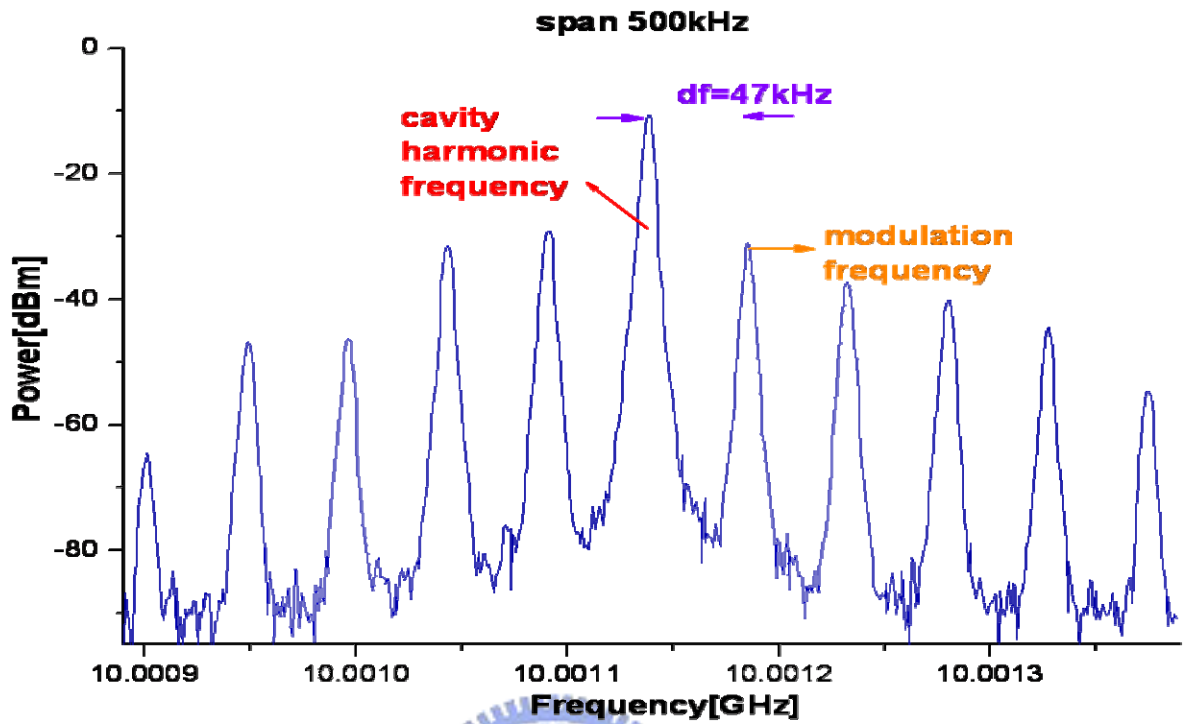


Fig. 3.6 The RF spectrum (span 500 kHz, deviation frequency: 47 kHz)

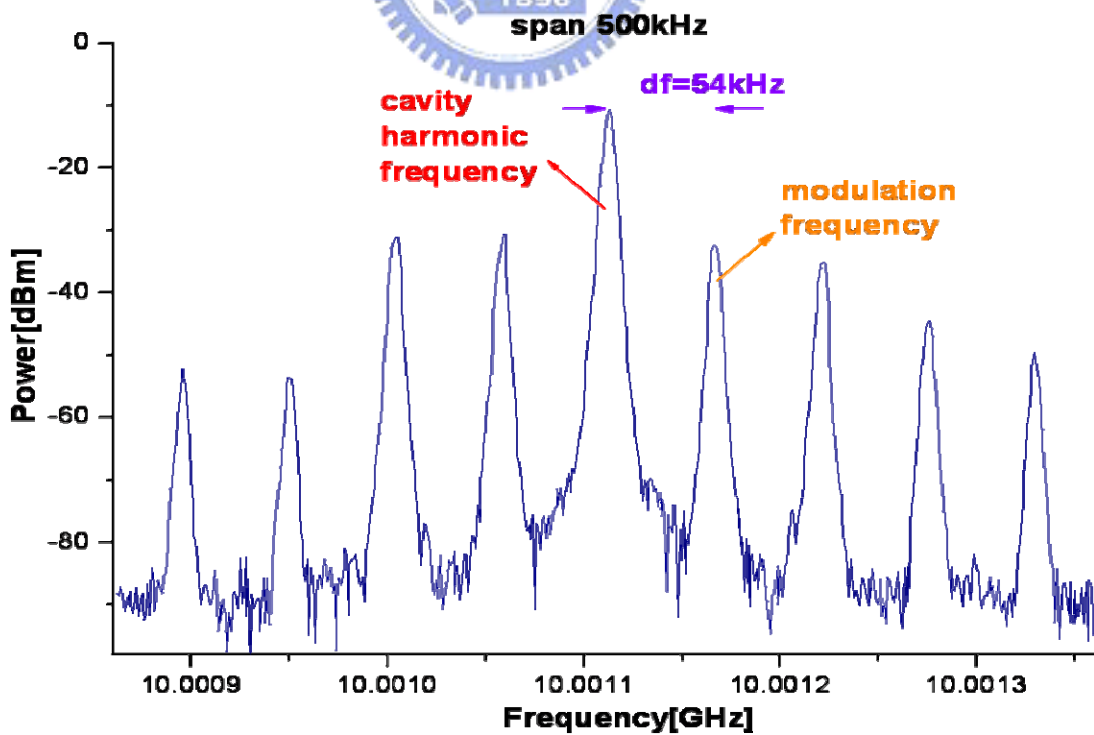


Fig. 3.7 The RF spectrum (span 500 kHz, deviation frequency: 54 kHz)

Finally, the pulsewidth of our laser is 0.6 ps. This is shown in figure 3.8.

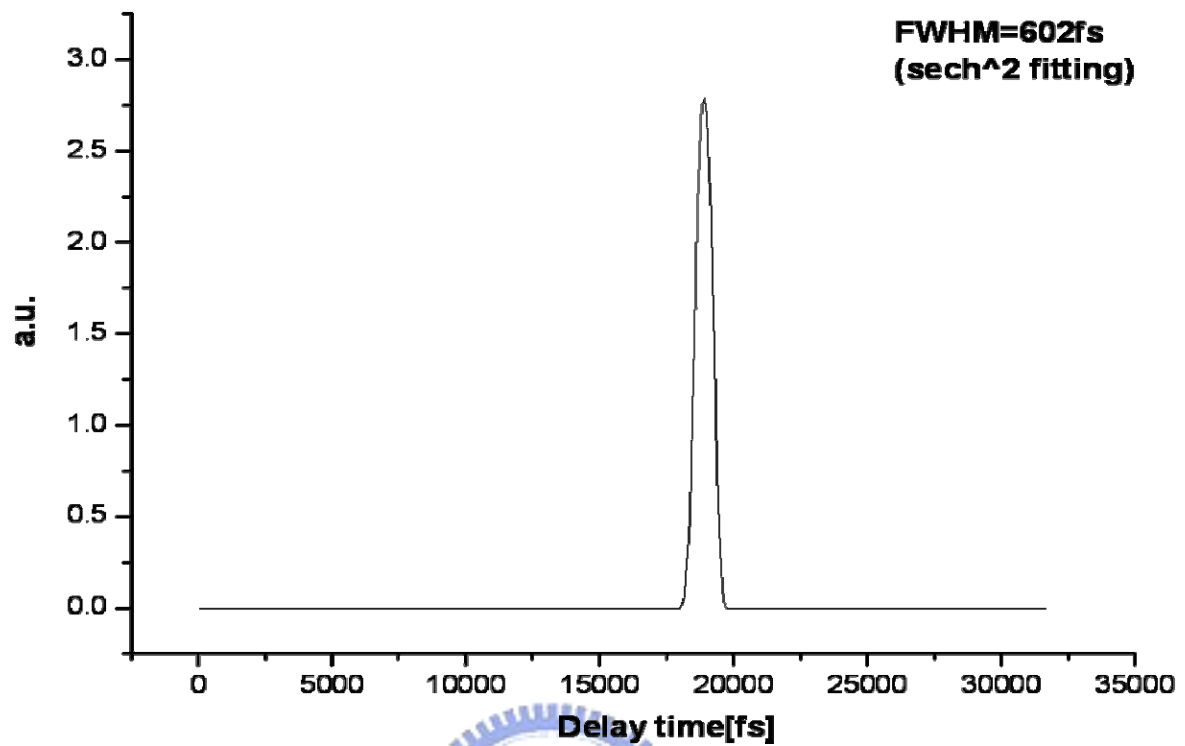


Fig. 3.8 Autocorrelation of the pulses



3.2 Pulse dynamics of ASM fiber soliton lasers

3.2.1 Variational analysis

We know that an asynchronously mode-locked fiber soliton laser [3.1] can be described by the master equation as follows:

$$\frac{\partial u(T, t)}{\partial T} = \left(\frac{g_0}{1 + \frac{\int |u|^2 dt}{E_s}} - l_0 \right) u + (d_r + jd_i) \frac{\partial^2 u}{\partial t^2} + (k_r + jk_i) |u|^2 u + jM \cos[\omega_m (t + \Delta T(T))] \quad (3.1)$$

where $u(T, t)$ is the complex field envelope, g_0 is the unsaturated gain, E_s is the saturation energy, l_0 is the loss, d_r is the effect of an optical filter, d_i is group velocity dispersion, k_r is the effect of polarization additive pulse model-locking (P-APM), k_i is self phase modulation, M is the depth of the phase modulation, ω_m is the modulation angular frequency of the phase modulator, T is the number of round trip, t is the time axis measured in the moving frame of the pulse propagating at the group velocity, and $\Delta T(T)$ is the timing deviation between the center of the pulses and the modulation signal. The pulse $u(z, t)$ in the laser is asynchronously modulated by a phase modulator with the modulation frequency $f_M = \frac{\omega_m}{2\pi}$, which is detuned from the cavity harmonic frequency f_H by a deviation frequency Δf in the range of 10-60 kHz. We adopt the reasonable solution ansatz described below,

$$u(T, t) = a(T) \operatorname{sech} \left[\frac{t - t_0(T)}{\tau(T)} \right]^{1+j\beta(T)} e^{j[\omega(T)(t-t_0(T))+\theta(T)]} \quad (3.2)$$

where $a(T)$ is the pulse amplitude, $\tau(T)$ is the pulse width, $t_0(T)$ is the pulse center position, $\beta(T)$ is the chirp, $\omega(T)$ is the pulse center frequency, and $\theta(T)$ is the pulse phase. The variational method is applied to solve Equation (3.1) and the

evolution equations for pulse parameters are obtained in Equation (3.2). Figure 3.9(a)-(b) shows the simulation results of the pulse timing position and the pulse center frequency for a particular case. The ratio of the cavity roundtrip frequency f_c to Δf is 400 and f_H is the 1000th harmonic of the cavity ($f_H = 1000f_c$). The other parameters are estimated based on our experimental observation that the output pulses are transform-limited (chirpless) and other measured results. They are $g = \frac{4}{1+5a^2(z)\tau(z)}$, $l=1$, $d_r=0.25$, $d_i=0.5$, $k_r=0.5$, $k_i=1$, and $M=1$. These values should be not far from the actual operating conditions of our laser. We can observe the slow periodic variations at the deviation frequency as shown in figure 3.9(a) and 3.9(b). Besides these two parameters, other pulse parameters are also found to exhibit smaller but more complicated slow periodic variation. The evolution of the pulse energy and the pulse-width are shown in figure 3.9(c) and 3.9(d) respectively, which clearly indicates that the oscillation is not purely sinusoidal. Direct numerical simulation has also been performed to verify the results.

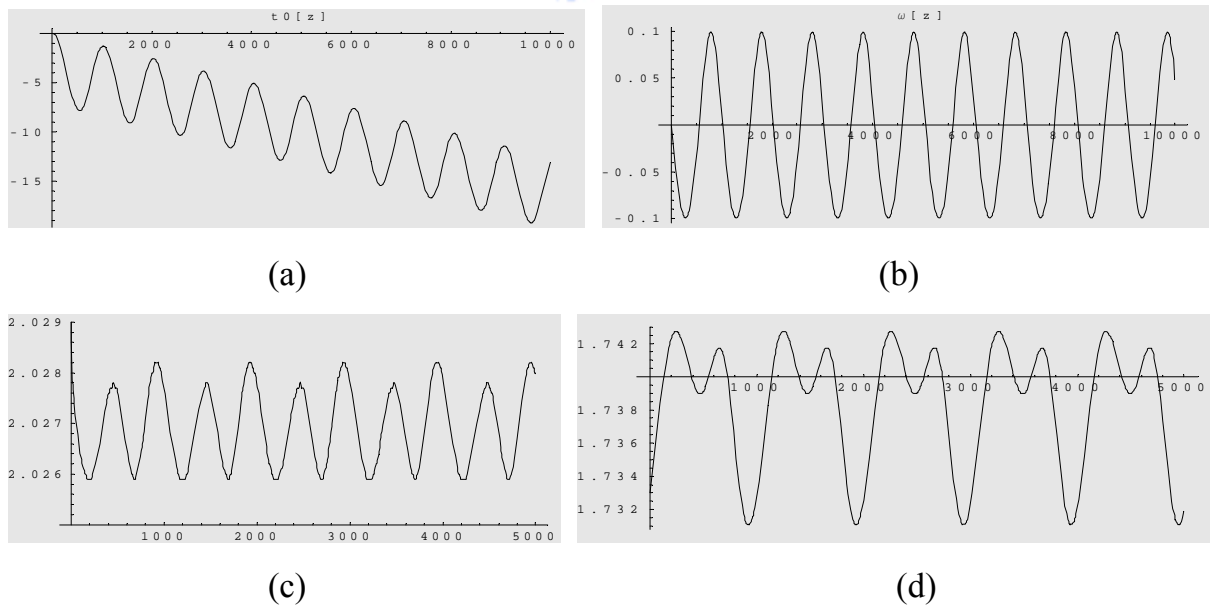


Fig. 3.9 Slow periodic evolution of the pulse parameters: (a) pulse timing position, (b) pulse center frequency, (c) pulse energy, (d) pulse-width.

3.2.2 Determination of periodic pulse timing position variation from RF spectra

For a soliton propagating in an asynchronously mode-locked Er-fiber laser, we have known that the pulse timing will exhibit slow periodic evolution, which can be obtained by the soliton perturbation theory [3.1] or the variational analysis. It can be written as:

$$s(T) \approx \delta t_0 \sin(\Delta\Omega T) \quad (3.3)$$

In the experiment, the detected pulse train signals from the fast photodetector can be expressed as:

$$i(t) = [r(t) \otimes p(t)] \otimes \sum_{m=-\infty}^{m=\infty} \delta[t - mT_H + \delta t_0 \sin(\Delta\omega mT_H)] \quad (3.4)$$

where $r(t)$ is the response of the fast photodiode, $p(t)$ is the pulse intensity, and T_H is the period of the cavity harmonic, δt_0 is the timing displacement of sinusoidal variation, and \otimes stands for the convolution. This is shown in figure 3.10.

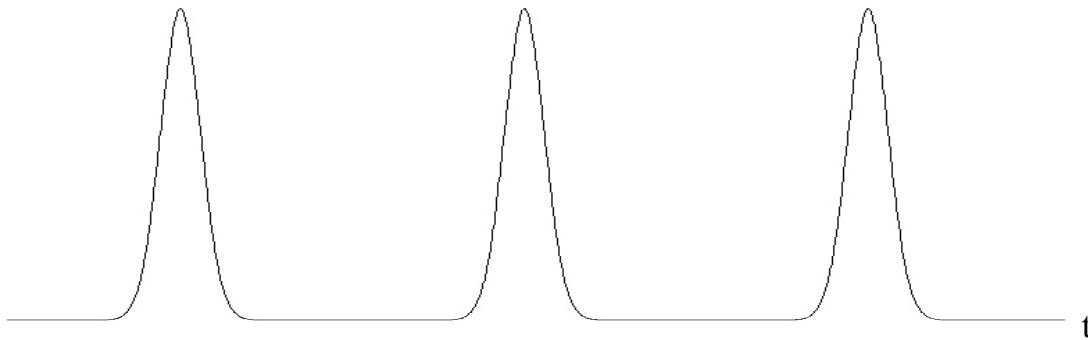


Fig. 3.10 The pulse train signals in the time domain

We have assumed that the pulse timing deviation is approximately sinusoidal and the pulse width is much shorter than the response function $r(t)$ of the photodiode. The Fourier transform of $p(t)$ can be shown to be:

$$\begin{aligned}
F\{i(t)\} &= F\{r(t)\}F\{p(t)\}F\left\{\sum_{m=-\infty}^{m=\infty} \delta(t - mT_H + \delta t_0 \sin(\Delta\omega mT_H))\right\} \\
&\propto r(\omega)p(\omega) \sum_{n=-\infty}^{n=\infty} J_n(\omega\delta t_0) \sum_{m=-\infty}^{m=\infty} \delta(\omega - m\omega_H + n\Delta\omega) \quad (3.5)
\end{aligned}$$

where $r(\omega)$ and $p(\omega)$ are the Fourier transform of the response of the fast photodiode and the pulse intensity respectively. This is shown in figure 3.11.

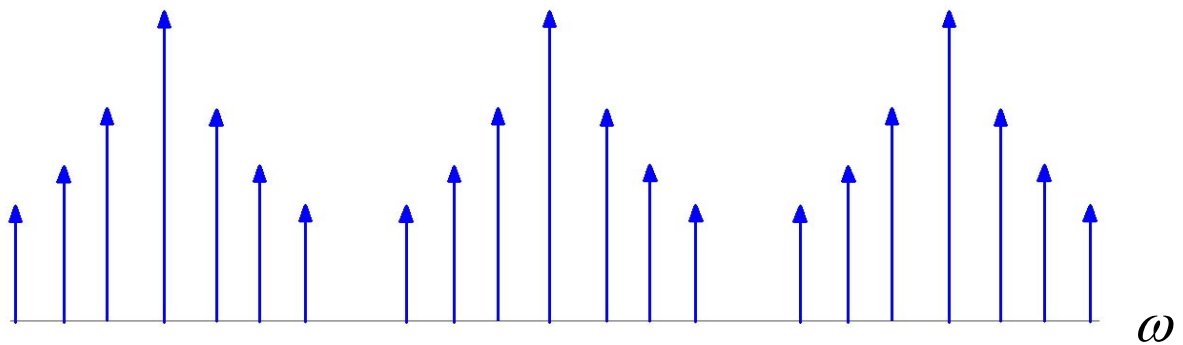


Fig. 3.11 The pulse train signals in the frequency domain

Therefore the periodic variation of the pulse timing position will produce the frequency sub-components on the RF spectrum. The frequency sub-components obtained from the fast photodiode are amplified by an amplifier, and finally are displayed on the RF spectrum analyzer. This is shown in figure 3.12.

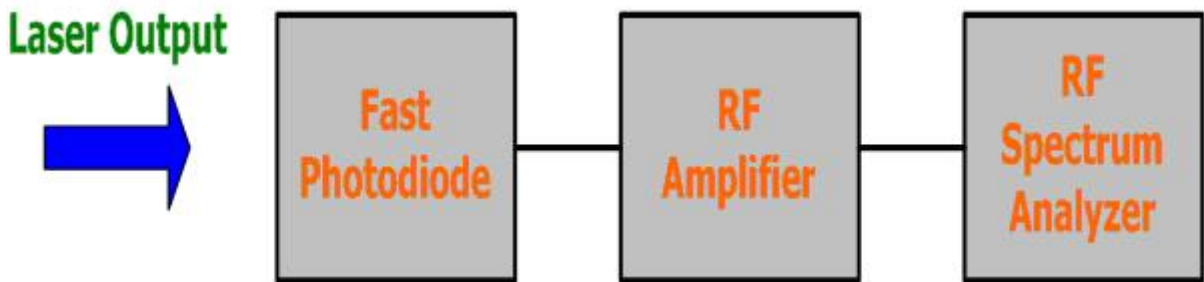


Fig. 3.12 Schematic of observed the frequency sub-components

The intensity at the frequency $\omega = 2\pi(mf_H + n\Delta f)$ observed in the RF spectrum is expected to be proportional to $|J_n(\omega t_0)|^2$. We calculate the ratio of 0th (the cavity

harmonic frequency) and 1st (the modulation frequency) sub-components for m=1(see the figure 3.13). It can be written as:

$$\Delta = \left| \frac{J_0(\omega_H \delta t_0)}{J_1[(\omega_H + \Delta\omega)\delta t_0]} \right|^2 \cong \left| \frac{J_0(\omega_H \delta t_0)}{J_1(\omega_H \delta t_0)} \right|^2 \quad (3.6)$$

Finally, the value of δt_0 can be determined.

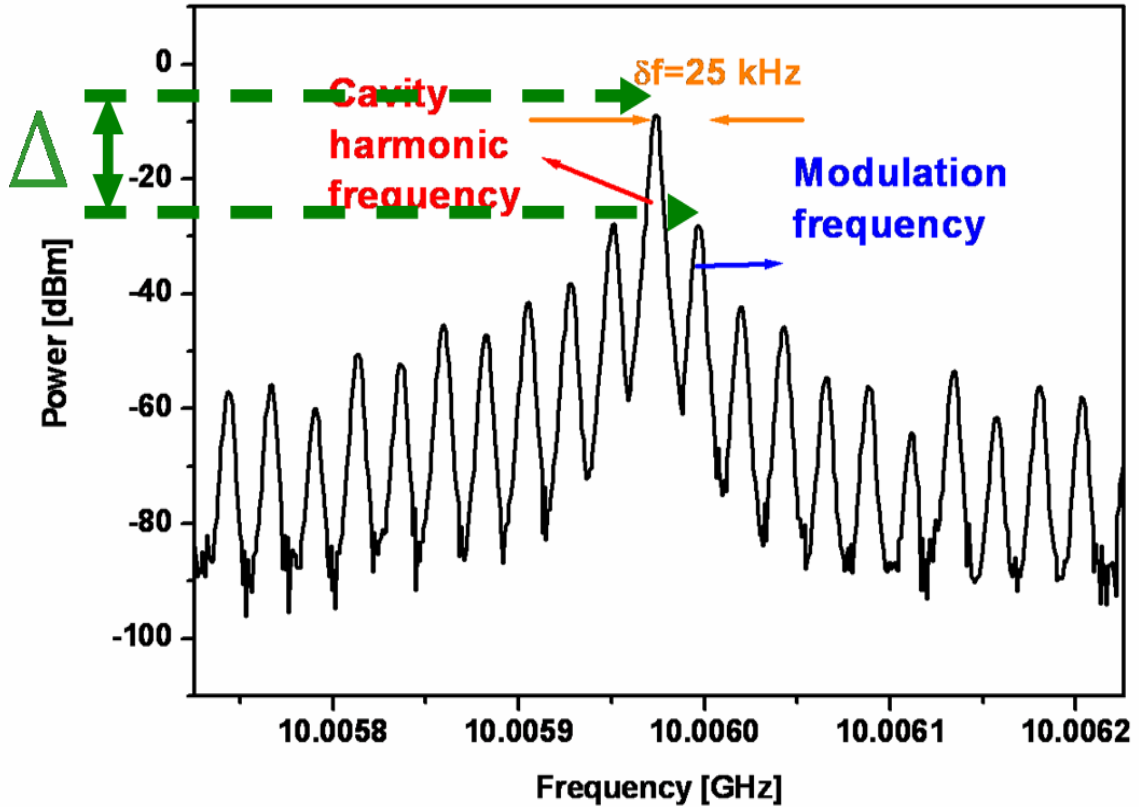


Fig. 3.13 The frequency sub-components on the RF spectrum

We want to prove that the experimental results are consistent with the theory, so we use Equation (3.6) to calculate the ratio for the four harmonic components from 10 GHz to 40 GHz. With a smaller span of 750 kHz in our experiment, the RF spectra of 10 GHz to 40 GHz are shown in figure 3.14 to 3.17. The experimental parameters are list in table 3.2.

Input parameters	
980 nm pump	L:602 mA ; R:350 mA
cavity length	24.84 m
mode spacing	8.3 MHz
repetition rate	10.0218258 GHz
modulation strength	23 dBm
Results	
central frequency	1547.06 nm
SMSR	70.17 dB
output power	20 mW
optical spectrum	4.9 nm
bandwidth	
deviation frequency	53 kHz

Table 3.2 The parameters of the mode-locked laser

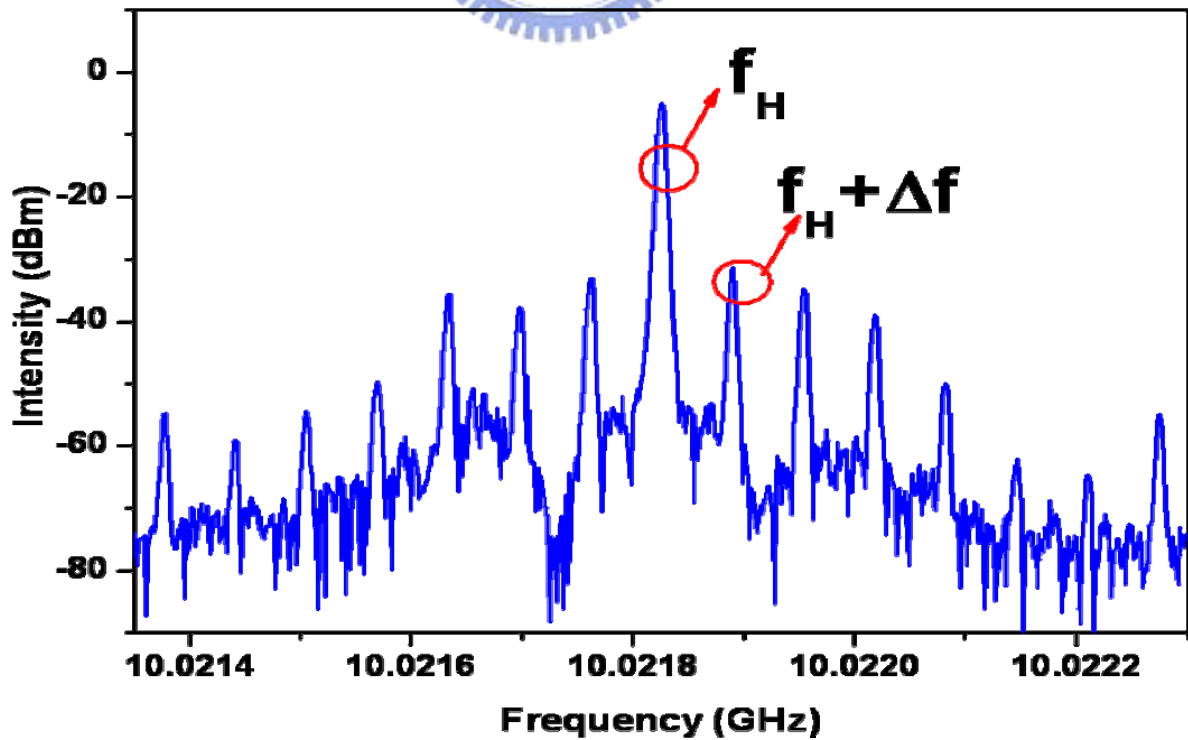


Fig. 3.14 RF spectrum near 10 GHz (Span: 750 kHz)

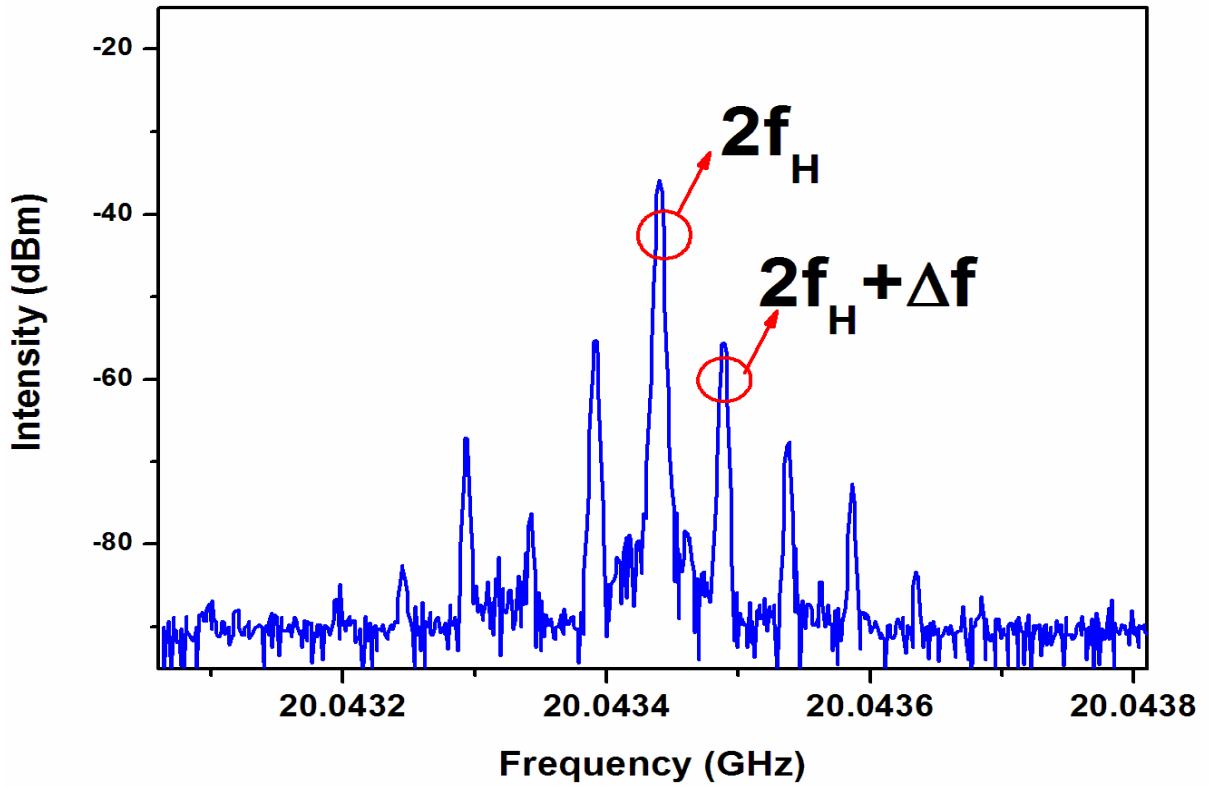


Fig. 3.15 RF spectrum near 20 GHz (Span: 750 kHz)

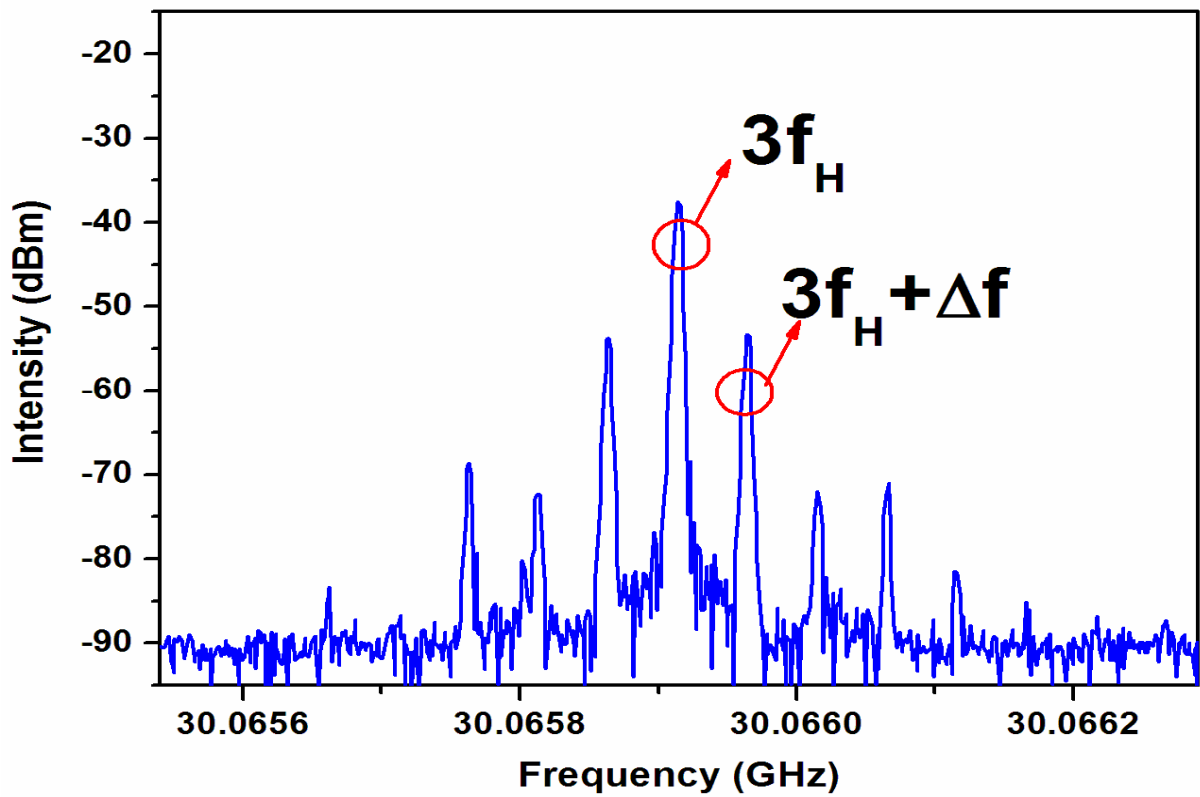


Fig. 3.16 RF spectrum near 30 GHz (Span: 750 kHz)

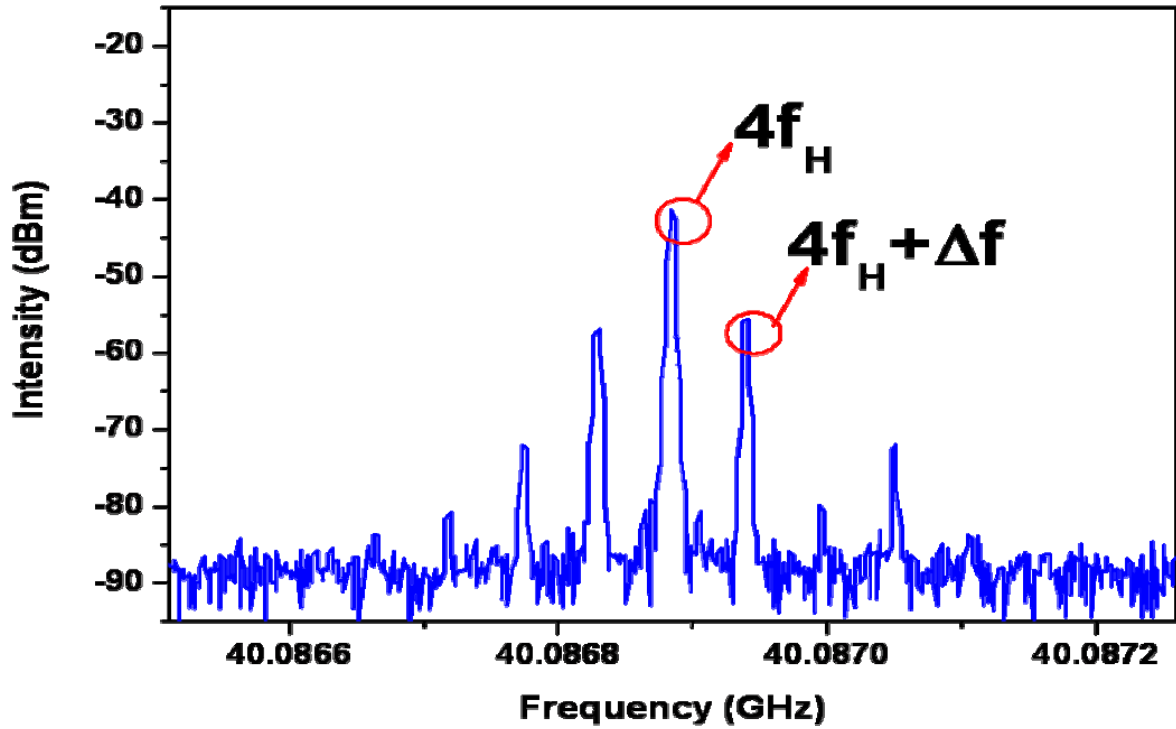
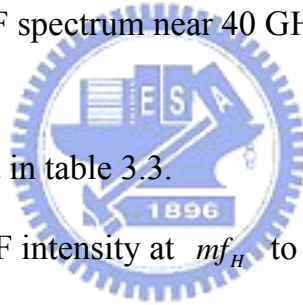


Fig. 3.17 RF spectrum near 40 GHz (Span: 750 kHz)



The calculated results are list in table 3.3.

Table 3.3 The ratios of the RF intensity at mf_H to that at $mf_H + \Delta f$ from m=1 to m=4

	RF intensity I_A at mf_H (dBm)	RF intensity I_B at $mf_H + \Delta f$ (dBm)	$I_A - I_B$ (dBm)	$20 \text{Log} \left[\frac{J_0(mx)}{J_1(mx)} \right]$ (dB) $x = 0.09474$	
10 GHz	m=1	-5.25	-31.72	26.48	26.48
20 GHz	m=2	-36.21	-55.23	19.02	20.43
30 GHz	m=3	-37.63	-53.4	15.77	16.86
40 GHz	m=4	-41.46	-55.75	14.29	14.29

The calculated ratios by assuming $x = \omega_H \delta t_0 = 0.09474$ or $\delta t_0 = 1.5$ ps are listed in the last column of Table 3.3, which is quite close to the experimental data in the adjacent column. This proves the consistency of our estimation.

3.2.3 Determination of periodic pulse center frequency variation from RF spectra

We already know that the pulse center frequency also exhibits the slow periodic variations in an asynchronously mode-locked Er-fiber laser. To determine the frequency variation experimentally, we propagate the pulses from the laser through a section of SMF-28 fiber and compare the timing variation before and after the SMF fiber. To be proved below, the pulse center frequency variation can then be estimated by the following formula:

$$\Delta\lambda = \frac{\sqrt{(\delta t_{02})^2 - (\delta t_{01})^2}}{LD} \quad (3.7)$$

Where δt_{01} / δt_{02} : periodic pulse timing position variation before/after the SMF 28 fiber

$\Delta\lambda$: periodic pulse center frequency variation

D: dispersion parameter of SMF 28

L: length of SMF 28

From the theory we know that the pulse center frequency variation is 90° out of the phase with the pulse timing position. Therefore the induced timing variation through the dispersion of the SMF fiber will also be out of the phase with the original timing variation. This is shown in figure 3.18.

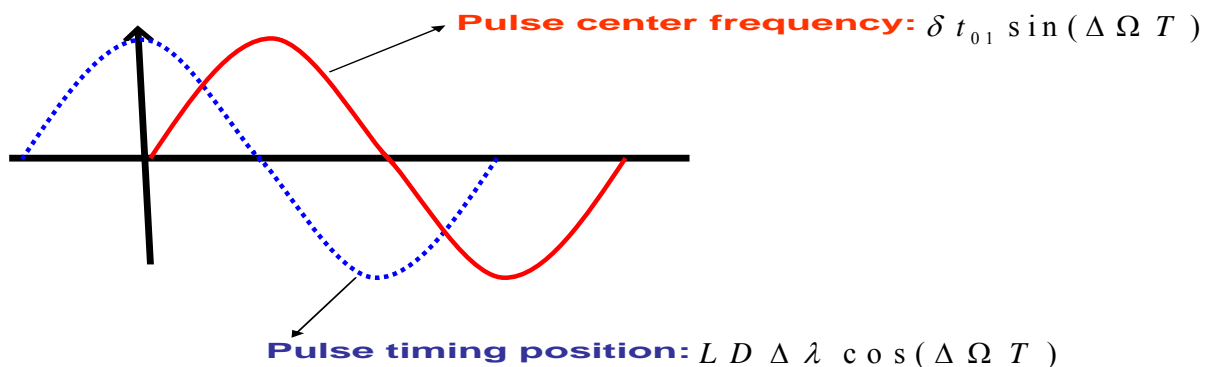


Fig 3.18 Schematic of pulse center frequency and pulse timing position variation

Therefore, we can use this relationship to derive Equation (3.7). It is easy to show that:

$$\begin{aligned}
 & \delta t_{01} \sin(\Delta\Omega T) - LD\Delta\lambda \cos(\Delta\Omega T) \\
 & = \delta t_{02} \sin(\Delta\Omega T - \varphi) \\
 & \delta t_{02} = \sqrt{(\delta t_{01})^2 + (LD\Delta\lambda)^2} \\
 \Rightarrow \Delta\lambda & = \frac{\sqrt{(\delta t_{02})^2 - (\delta t_{01})^2}}{LD}
 \end{aligned} \tag{3.8}$$

The periodic variations of the pulse center wavelength $\Delta\lambda$ will produce the timing variation proportional to $D \times L \times \Delta\lambda$ with D being the fiber dispersion, L being the fiber length. The out-of-phase characteristics give rise to the expression in (3.8) and in turns lead to (3.7).

In our experiment, we can analyze the RF spectra without and with the SMF 28 to get the pulse timing position variation, and then use Equation (3.7) to calculate the periodic pulse center frequency variations. This is shown in figure 3.19.

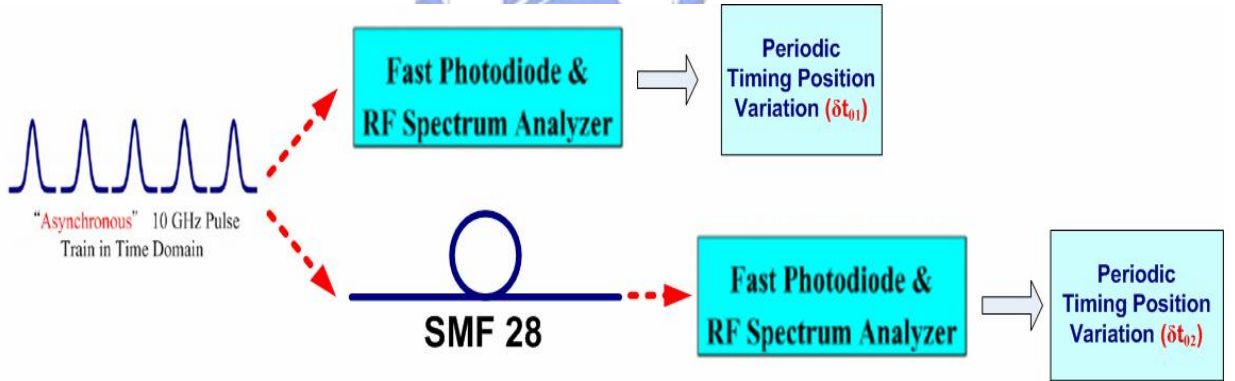


Fig 3.19 Schematic of measuring the pulse timing position variation without and with the SMF 28 fiber

So we observe the RF spectra at 10 GHz with the length of SMF-28 fiber being 0 m, 50 m, 100 m, 200 m, and 300 m. A smaller RF span of 500 kHz is used in the measurement, the RF spectra are shown in figure 3.20 to 3.24. Then, the experimental parameters are list in table 3.4.

Table 3.4 The parameters of the mode-locked laser

Input parameters	
980 nm pump	L:602 mA ; R:450 mA
cavity length	24.84 m
mode spacing	8.3 MHz
repetition rate	10.0012375 GHz
modulation strength	21 dBm
Results	
central frequency	1564.05 nm
SMSR	71.17 dB
output power	20 mW
optical spectrum	3.45 nm
bandwidth	
deviation frequency	34.3 kHz

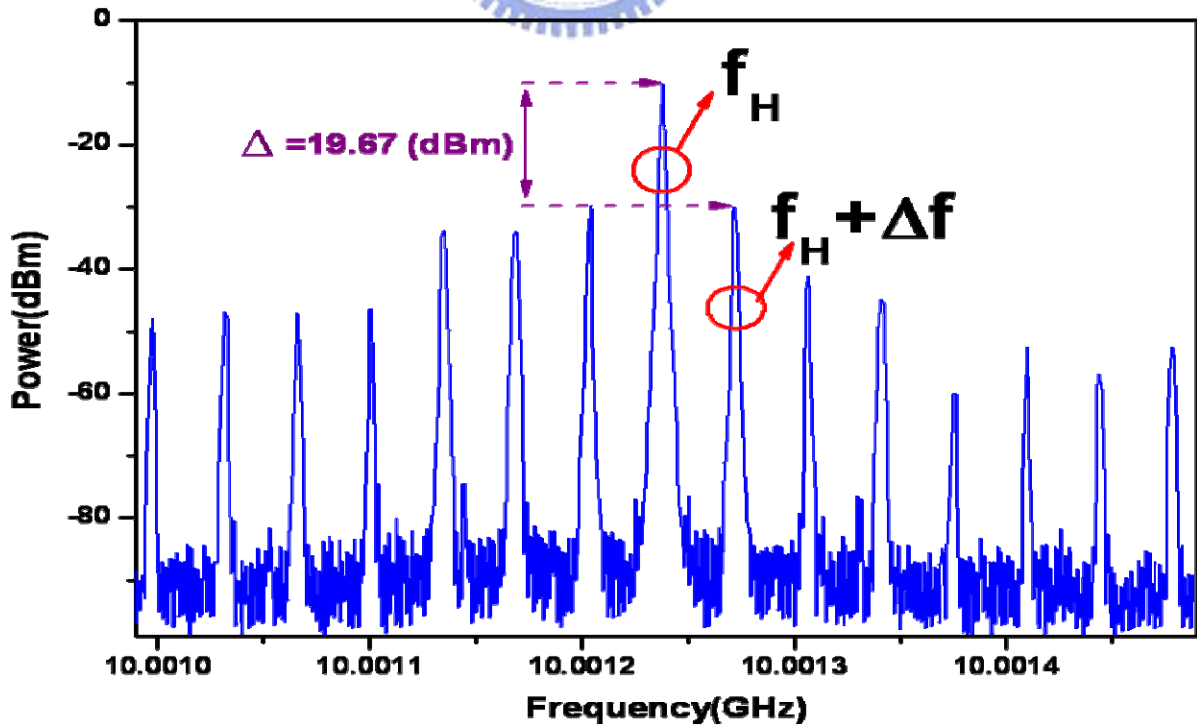


Fig. 3.20 RF spectrum near 10 GHz with 0 m SMF 28 fiber (Span: 500 kHz)

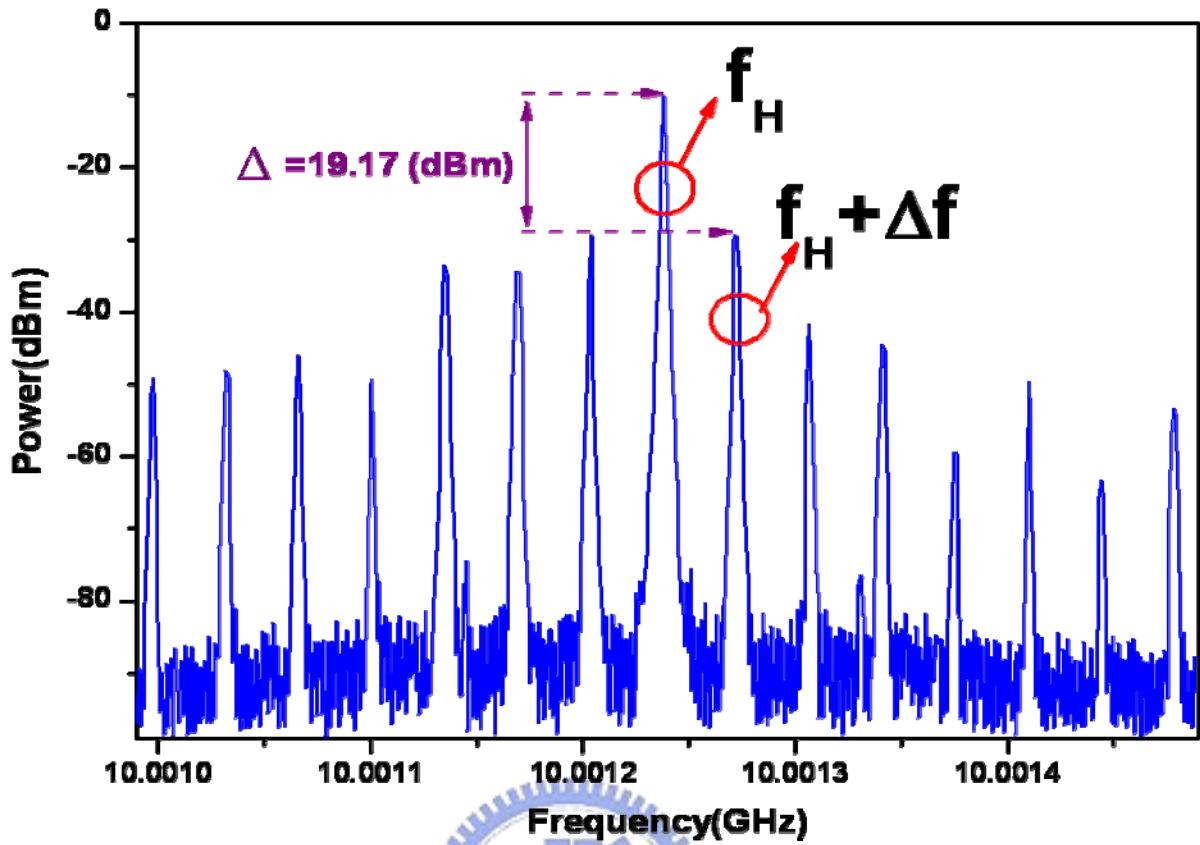


Fig. 3.21 RF spectrum near 10 GHz with 50 m SMF 28 fiber (Span: 500 kHz)

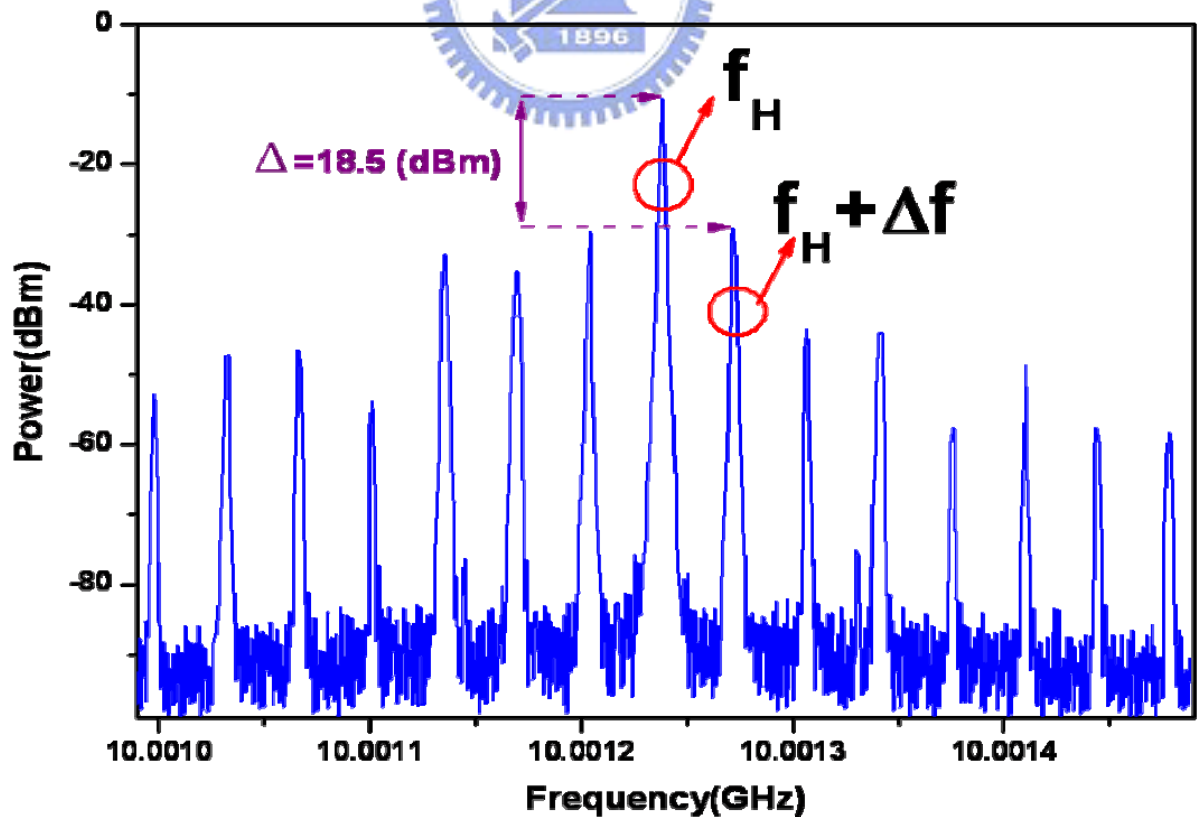


Fig. 3.22 RF spectrum near 10 GHz with 100 m SMF 28 fiber (Span: 500 kHz)

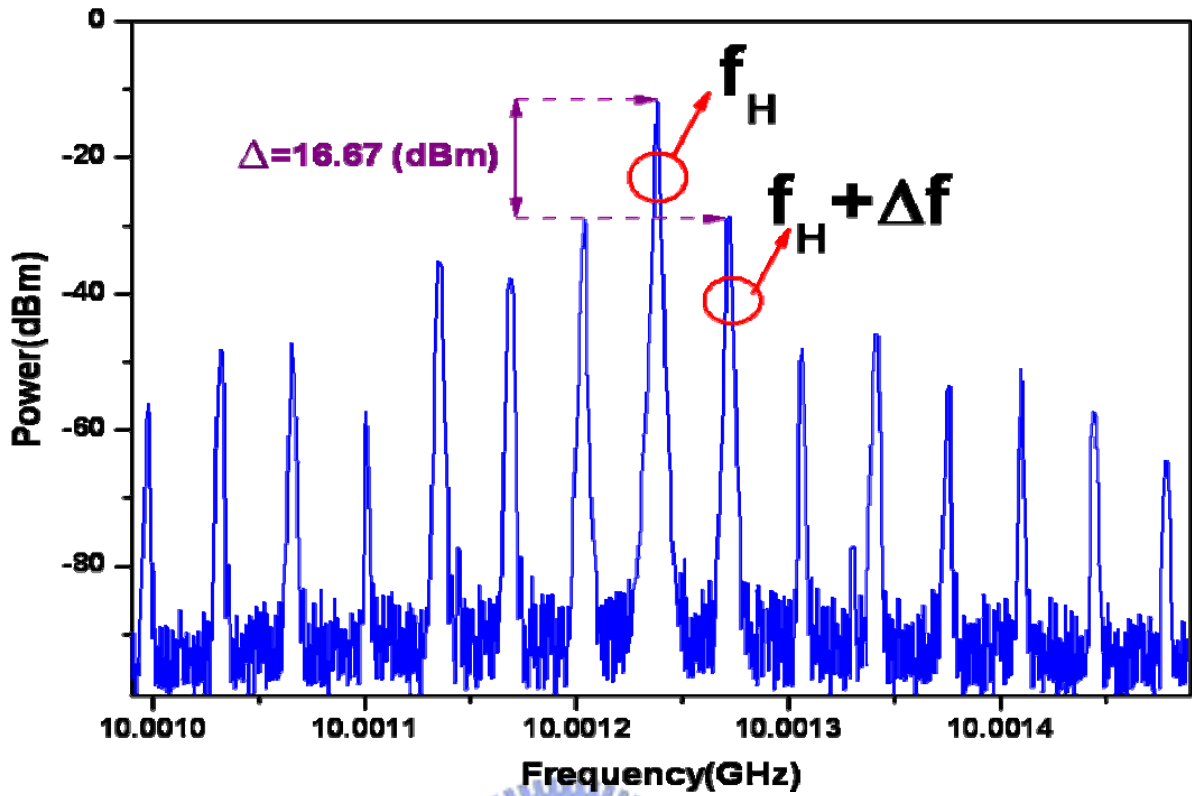


Fig. 3.23 RF spectrum near 10 GHz with 200 m SMF 28 fiber (Span: 500 kHz)

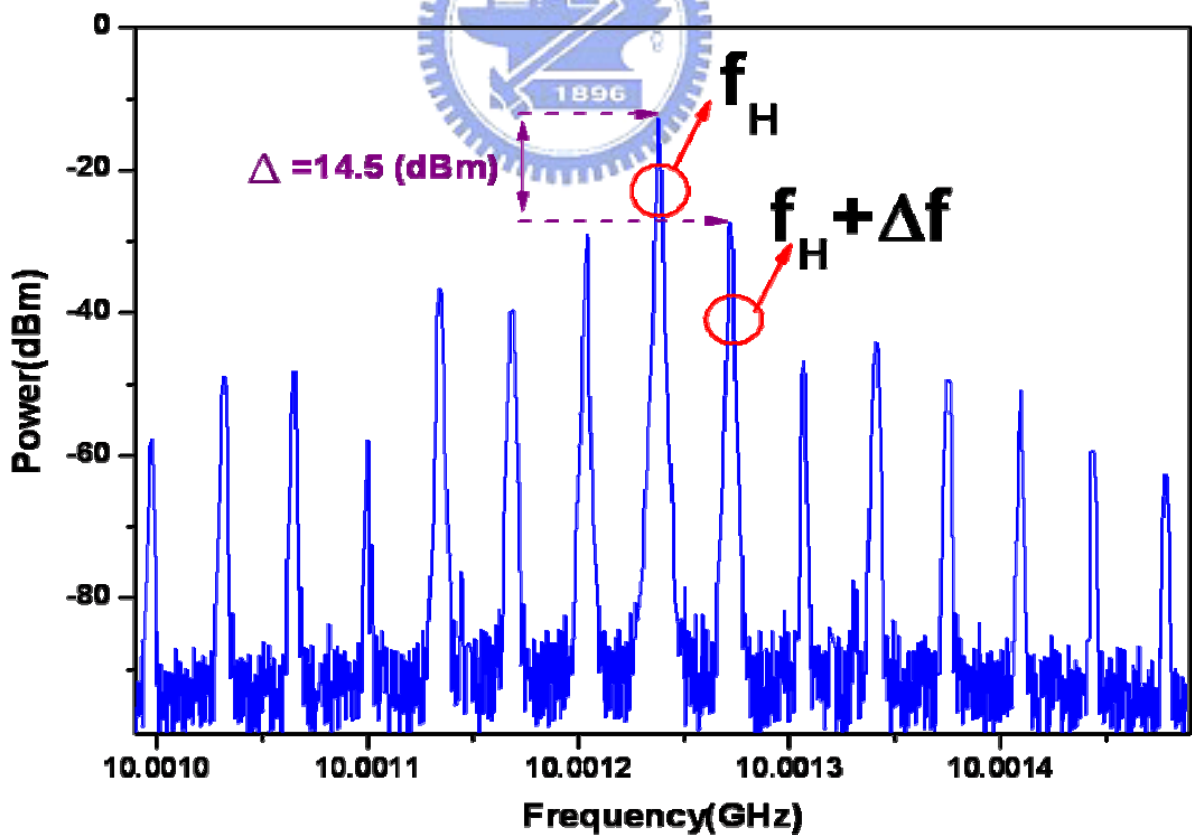


Fig. 3.24 RF spectrum near 10 GHz with 300 m SMF 28 fiber (Span: 500 kHz)

The experimental and calculated results are listed in table 3.5.

Table 3.5 The ratios of the RF intensity and the estimated wavelength variation

SMF 28 Length (m)	$\Delta=I_A-I_B$ (dBm)	δt_{oi} (ps)	$\Delta \lambda$ (nm)
0m	19.67	3.28868	
50m	19.17	3.48129	1.34343
100m	18.5	3.75671	1.06817
200m	16.67	4.62097	0.954771
300m	14.5	5.89252	0.958709

At first we measure the difference between I_A and I_B from 0 m to 300 m, and obtain the values of the Periodic Pulse Timing Position Variation. Then, we use the Periodic Pulse Timing Position Variation and Equation (3.7) to get the Pulse Center Frequency Variation. Finally, the Pulse Center Frequency Variation of $\Delta\lambda \approx 1.08 \text{ nm}$ is found in this particular case. This is actually a significant amount of wavelength variation and may find some interesting applications in fiber dispersion measurement or fiber sensors.

Reference

- [3.1] H.A. Haus, D.J. Jones, E.P. Ippen, and W.S. Wong, "Theory of soliton stability in asynchronous mode-locking," *IEEE J. Lightwave Technology* 14, 622, 1996.



Chapter 4

Conclusion

4.1 Summary

In the thesis work, the asynchronous mode-locked Er-fiber soliton fiber laser has been successfully studied. The laser can generate pulse trains with the repetition rate as high as 10 GHz and with the pulse width as short as 600 fs. The optical spectrum bandwidth is about 5.0 nm and the supermode suppression ratio (SMSR) is > 70 dB. The pulse shape from the SHG autocorrelation measurement looks very good. There are all due to the combination of P-APM, SPM, feedback control, sliding-frequency guiding filter, and asynchronous mode-locking mechanisms in a single fiber laser cavity to form a mode-locked fiber laser with good performance.

We have found a new method for characterizing experimentally the pulse timing position and the pulse center frequency variation. The method can be carried out by directly analyzing the RF spectra of the laser output. In our experiment, the periodic pulse timing position variation is about 1.5 ps and the pulse center frequency variation is about 1.14 nm, for the particular case we considered.

All the pulse parameters of the laser output exhibit slow periodic variation at the deviation frequency from our variational analysis. They include the pulse energy, pulse-width..., not just the timing position and center frequency as expected previously. The slow periodic variation of the pulse parameters is also not purely sinusoidal with a single frequency, but may be with small higher harmonic components. Although these higher harmonic components are relatively small when compared to the fundamental harmonic component, they may still show up in the electronic spectrum of the output pulse train.

4.2 Future work

We have found that the stability becomes an issue for our 10 GHz asynchronous mode-locked Er-fiber soliton fiber laser. More powerful stabilization mechanisms must be introduced to maintain the deviation frequency between the modulation and the cavity mode frequency. Although we have developed the feedback control good mechanism to stabilize the mode-locked laser and achieve the compensation of the cavity length for keeping the cavity mode frequency remained the same in our laser, it is still difficult to stabilize the frequency in the long term with chaotic temperature changes. A better external temperature controlling method for reducing the unpredictable variation should help to improve the stable operation of our laser.

